



Crystal orientation effects in $\delta^{18}\text{O}$ for magnetite and hematite by SIMS

Jason M. Huberty^{*}, Noriko T. Kita, Reinhard Kozdon, Philipp R. Heck¹, John H. Fournelle, Michael J. Spicuzza, Huifang Xu, John W. Valley

WiscSIMS and NASA Astrobiology Institute, Department of Geoscience, University of Wisconsin, 1215 W Dayton St., Madison, WI 53706, USA

ARTICLE INFO

Article history:

Received 18 February 2010

Received in revised form 11 June 2010

Accepted 21 June 2010

Editor: D.B. Dingwell

Keywords:

Magnetite

Hematite

SIMS

Oxygen isotopes

EBSD

Crystal orientation effects

ABSTRACT

In situ high precision analysis of oxygen isotope ratios ($\delta^{18}\text{O}$) by secondary ion mass spectrometry (SIMS) reveals that instrumental bias in $\delta^{18}\text{O}$ for magnetite varies due to crystal orientation effects. Multiple analyses of $\delta^{18}\text{O}$ have an average precision of $\pm 0.4\%$ (2SD) in single grains of magnetite, close to $\pm 0.3\%$, that obtained for multiple grains of UWQ-1, a homogeneous quartz standard. In contrast, the average precision is five to ten times worse, $\pm 2\text{--}3\%$ (2SD), from grain-to-grain of magnetite due to variation in instrumental bias with crystal orientation. Electron backscatter diffraction shows that individual grains of magnetite are single crystals and that crystal orientation varies randomly from grain-to-grain. The crystal orientation for each magnetite grain is plotted relative to the incident angle of the SIMS primary Cs^+ beam. High values of $\delta^{18}\text{O}$ are measured when the Cs^+ beam is parallel to $\langle uv0 \rangle$, from [110] to [100], preferred channeling and focusing directions for magnetite. Routine $\delta^{18}\text{O}$ analysis at WiscSIMS utilizes a Gaussian focused Cs^+ primary beam (deep-pit mode) at primary and secondary voltages of +10 kV and –10 kV respectively (total impact energy 20 keV). Four analytical experiments were conducted in attempts to improve the grain-to-grain precision in measured $\delta^{18}\text{O}$ for magnetite: (1) applying an energy offset of 50 eV, (2) using a Köhler illuminated beam (shallow-pit mode), (3) reducing the total impact energy, and (4) varying the primary and secondary accelerating voltages. The best results were obtained in experiment (4) at primary/secondary accelerating voltages of +3 kV/–10 kV respectively with an incident Cs^+ beam angle of 14° . The grain-to-grain precision in measured $\delta^{18}\text{O}$ for magnetite improves from $\pm 2.9\%$ to $\pm 0.8\%$ (2SD) at +10 kV/–10 kV and +3 kV/–10 kV analysis respectively, while precision in single grains is $\pm 0.4\%$ for both. Instrumental bias in $\delta^{18}\text{O}$ also varies with crystal orientation for hematite at similar levels as is seen for magnetite. The grain-to-grain precision in measured $\delta^{18}\text{O}$ for hematite improves from $\pm 2.1\%$ to $\pm 1.0\%$ (2SD) at +10 kV/–10 kV and +3 kV/–10 kV analysis respectively, while precision in single grains is $\pm 0.3\%$ (2SD) for both. Importantly, crystal orientation effects have not been identified at levels of $\pm 0.3\%$ for $\delta^{18}\text{O}$ in silicates or other minerals analyzed by WiscSIMS though many minerals remain to be examined.

© 2010 Elsevier B.V. All rights reserved.

1. Introduction

Magnetite (Fe_3O_4) is a common mineral in sedimentary, metamorphic, and igneous rocks. Oxygen isotope ratios ($\delta^{18}\text{O}$) in magnetite can provide important information on fluid conditions and temperatures during sedimentation, diagenesis, metamorphism, magmatism, and the genesis of iron ore deposits and banded iron formations (BIFs). The fractionation of oxygen isotopes between magnetite and quartz (SiO_2) is the most sensitive oxygen isotope geothermometer (Valley, 2001). Most studies of $\delta^{18}\text{O}$ for magnetite employed fluorination and gas-source mass spectrometry, either in

nickel reaction vessels, or by laser, while in situ secondary ion mass spectrometry (SIMS) analyses of $\delta^{18}\text{O}$ for magnetite have been limited to a relatively small number of studies of metamorphic rocks and chondritic meteorites (Valley and Graham, 1991, 1993; Eiler et al., 1995a,b; Choi et al., 1997, 1998; Yurimoto et al., 2008). However, growth zonation in magnetite is common, and in many rocks magnetite grains are small and scarce. Thus, the in situ capabilities of SIMS are potentially of great importance, and procedures for precise and accurate measurements are needed.

Isotope ratio analyses by SIMS typically show instrumental mass fractionation (IMF) and matrix effects, collectively termed instrumental mass bias. The magnitude of bias is mineral specific and varies with chemical composition, thus requiring the establishment of working curves for minerals with significant solid solution and the use of standards similar to samples in chemical composition (Hervig et al., 1992; Eiler et al., 1997; Riciputi et al., 1998; Valley and Kita, 2009). SIMS analyses are sometimes considered insensitive to crystal structure and orientation because the sputtering of high-energy

^{*} Corresponding author. Tel.: +1 608 262 8960; fax: +1 608 262 0693.

E-mail address: jason@geology.wisc.edu (J.M. Huberty).

¹ Present address: Robert A. Pritzker Center for Meteoritics and Polar Studies, Department of Geology, The Field Museum, 1400 S Lake Shore Dr, Chicago, IL 60605, USA and Chicago Center for Cosmochemistry, The University of Chicago, 5734 S Ellis Ave., Chicago, IL 60637, USA.

primary ions is thought to destroy the upper 5 to 10 nm of the crystal structure of the sample (Benninghoven, 1994). Eiler et al. (2007) reported no detectable difference in instrumental bias of $\delta^{18}\text{O}$ between albite and glass with a similar composition. To date, about 50 minerals have been characterized as isotope standards at WiscSIMS by mounting multiple grains at random orientations, and for these minerals, no variation in bias due to crystal orientation effects has been detected (Valley and Kita, 2009).

Crystal orientation effects in $\delta^{18}\text{O}$ for magnetite by SIMS have been previously suggested by Lyon et al. (1998). Those authors analyzed two magnetite samples (LP204-1 and SC1) with an Isolab 54, and reported a precision of $\pm 5\%$ (2SD) at varying crystal orientation and a precision of $\pm 2\%$ (2SD, $n = 22$) in a single grain of magnetite LP204-1. One euhedral magnetite crystal (SC-1) was analyzed with the (111) plane, the octahedral face, mounted parallel to the polished surface. The mount was analyzed in multiple crystal orientations by rotating it in the SIMS sample holder through a range of 290° about the [111] direction (parallel to the secondary beam), and high $\delta^{18}\text{O}$ values were found at $\sim 120^\circ$ intervals. Lyon et al. (1998) suggested high $\delta^{18}\text{O}$ values were measured when the primary Cs^+ beam was parallel to the set of directions $\langle 110 \rangle$ in magnetite.

Lyon et al. (1998) is the only prior study reporting crystal orientation effects for $\delta^{18}\text{O}$ by SIMS. Until now, these results seemed contradictory to earlier studies using different instruments (CAMECA IMS-3f, -4f) where randomly oriented crystals of magnetite (including LP204-1) yielded a spot-to-spot reproducibility of $\pm 2\text{--}3\%$ (2SD) (Valley and Graham, 1991, 1993; Hervig et al., 1992; Eiler et al., 1995a,b, 1997; Riciputi et al., 1998), indicating that any crystal orientation effect was less than half of that reported by Lyon et al. (1998). More recently, crystal orientation effects have been reported for measured values of $\delta^{56}\text{Fe}$ in magnetite (Kita et al., 2010), $\delta^{34}\text{S}$ in sphalerite (ZnS) and galena (PbS) (Kozdon et al., 2010), and $^{238}\text{U}/^{206}\text{Pb}$ ratios in baddeleyite (ZrO_2) (Wingate and Compston, 2001; Schmitt et al., 2010).

Recent improvements in SIMS instrumentation and refined analytical procedures, which include tuning and operation of the instrument, sample preparation, and standardization, have led to better precision in $\delta^{18}\text{O}$ of $\pm 0.2\text{--}0.3\%$ (2SD) for silicates and other minerals (Kita et al., 2009; Valley and Kita, 2009), but similar improvements were not obtained for magnetite. In an effort to develop high-precision sub-‰ analyses of $\delta^{18}\text{O}$ for magnetite by SIMS, we evaluated seven magnetite samples including LP204-1, a standard previously reported to be homogeneous in $\delta^{18}\text{O}$ at a precision of $\pm 2\%$ (2SD) (Valley and Graham, 1991, 1993; Hervig et al., 1992; Eiler et al., 1995a,b, 1997; Choi et al., 1997, 1998; Choi et al., 2000; Greenwood et al., 2000; Choi and Wasson, 2003; Hsu et al., 2006). Because these studies did not obtain sub-‰ precision for individual analyses, crystal orientation effects at this level of precision were not evaluated.

In this study, we used a CAMECA IMS-1280 large radius multi-collector SIMS to evaluate magnetite samples for homogeneity in oxygen isotope ratios. Electron backscatter diffraction (EBSD) was employed to determine the crystal orientation of each magnetite grain that was analyzed by SIMS. The goals of this study are to assess how crystal orientation affects measured values of $\delta^{18}\text{O}$, to correlate crystal orientation and measured $\delta^{18}\text{O}$, to improve the precision and accuracy of $\delta^{18}\text{O}$ for magnetite by SIMS, and to understand the physical processes behind variation in instrumental bias caused by crystal orientation effects.

1.1. Crystal orientation effects in the sputtering process

SIMS is one of a range of techniques whereby a sample is bombarded by an energetic primary ion beam and material is sputtered from the sample surface for analysis. Sputtering occurs when the collision of primary ions with target atoms creates atomic recoils in the sample, and these recoils create sustained collision cascades. Sputtering modifies the surface morphology of the sample and ions, neutral atoms, and molecules are ejected. Ion production is generally less than 10% of the total sputtered material for many elements (Behrisch and Eckstein, 2007). For SIMS, secondary O^- ion production from oxides and silicates is relatively high under sputtering by a Cs^+ primary beam, and the useful yield is close to 10% using a large radius magnetic sector SIMS with optimized instrumental parameters (Kita et al., 2009). Instrumental bias results from sputtering induced interactions in the sample and during the subsequent ionization, extraction, transmission, and detection of secondary ions (Riciputi et al., 1998; Valley and Kita, 2009).

Crystal orientation effects on the sputtered yield, secondary ion counts, and secondary ion energies for single crystals of metals and semiconductors are well known and an active field of study (Robinson, 1981; Behrisch and Eckstein, 2007; Eckstein, 2007). The most important effects to consider for SIMS are channeling of primary ions and focusing of secondary ions. Fig. 1 illustrates how crystal orientation effects might occur during SIMS analysis. A schematic cross-section through a crystalline sample is shown where the (110) planes of atoms, preferred crystal orientations for cubic crystals, are aligned parallel to the incident Cs^+ beam direction. Channeling takes place when some of the primary ions are directed between planes of atoms, e.g., (110), aligned parallel to the beam direction and buried at depth in the sample (Fig. 1a). Channeled ions do not contribute to sputtering and thus result in a lower secondary ion yield (Benninghoven et al., 1987).

Focusing of secondary ions, by contrast, occurs when atomic recoils in the sample initiate collision cascades termed focusing collision sequences. Momentum from the atomic recoils and secondary ions transferred into or between planes of atoms, resulting in

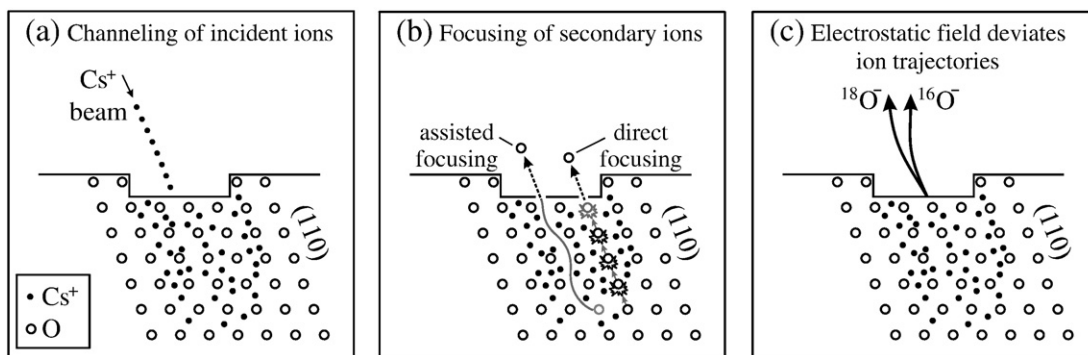


Fig. 1. Schematic cross-section through a crystalline sample with the (110) planes of atoms aligned parallel to the incident Cs^+ beam. (a) Channeling happens when some of the primary ions are directed between planes of atoms and buried at depth in the sample. (b) Focusing occurs when momentum and ions are transferred into or between planes of atoms, resulting in preferential emission of secondary ions. (c) We hypothesize that secondary ions emitted along channeling and focusing directions may have their trajectories deviated by the electrostatic field and could preferentially select the light isotope (^{16}O).

preferential emission of secondary ions along the same preferred crystal orientations, e.g., (110), as for channeling (Fig. 1b). Direct focusing takes place when momentum is transferred within or along planes of atoms, whereas assisted focusing occurs when cascading ions are directed between planes of atoms (Fig. 1b; Benninghoven et al., 1987).

Channeling and focusing have also been found to influence the angular distribution of secondary ions (Gnaser, 2007). Similarly, surface topography can deform the equipotential surfaces of the electrostatic field parallel to the sample surface, which in turn deviate the path of secondary ions (Kita et al., 2009). During SIMS analysis, secondary ions are accelerated by the voltage potential between the sample surface and the extraction plate 5 mm above the sample. We hypothesize that secondary ions emitted along focusing directions may have their trajectories similarly deviated by the electrostatic field and that this process could preferentially select the light isotope (^{16}O) (Fig. 1c).

Crystal orientation effects during sputtering primarily occur for minerals and phases with cubic crystal structures, which can be simple (e.g., pyrite, FeS_2), face-centered (e.g., magnetite), body-centered (e.g., CsCl), or diamond-centered (e.g., sphalerite, ZnS). Channeling and focusing effects are highest when the primary ion beam is parallel to the set of directions: $\langle uv0 \rangle$, from [110] to [100], for face-centered cubic; $\langle uww \rangle$, from [111] to [100], for body-centered cubic; and $\langle uuw \rangle$, from [111] to [110], for diamond-centered cubic crystal structures (Gnaser, 2007).

Fig. 2 shows perspective renderings of the crystal structure of magnetite using CrystalMaker® 8.2 (CrystalMaker, 2008). Thin black lines indicate one unit cell (32 oxygen atoms). Iron atoms are shown as black circles, oxygen atoms as white circles, and atomic bonds are omitted. Figs. 2a and b show the crystal structure of magnetite viewed parallel to [110] and [211] respectively, examples of channeling and focusing directions in magnetite. In these diagrams, rows of oxygen atoms are aligned in planes parallel to the viewing direction (perpendicular to the page). For comparison, Fig. 2c shows the crystal structure of magnetite viewed parallel to [543], a non-channeling direction, where planes of oxygen atoms are inclined relative to the viewing direction.

2. Samples and preparation

Seven magnetite samples were examined to identify a homogeneous oxygen isotope standard for SIMS analysis. Six samples are from the collections of the Department of Geoscience at the University of

Wisconsin-Madison: 5830, 5835, 5847, 08M2, 08-BI-12, and LP204-1; and one sample is from the Geological Survey of Japan: M34572-A. All samples are coarse-grained and magnetite-rich. The geologic setting of magnetites 5835, 5847, 08M2, and M34572-A are not known. Magnetite 5830 is from Lake Champlain (Adirondacks), New York, with no further information. Magnetite 08-BI-12 was collected from the lower cherty member of the Biwabik Iron Formation, Cleveland-Cliffs Mine, Babbitt, Minnesota, within 50 m of the contact with the Duluth Gabbro and is located within the orthopyroxene zone (Valaas Hyslop et al., 2008). Magnetite LP204-1 is from a hand sample of marble collected in float at Westin Mines within 30 m of the contact of the Marcy Anorthosite Massif in the central Adirondack Highlands (Valley and O'Neil, 1984). LP204-1 has been evaluated as a SIMS standard with a precision in $\delta^{18}\text{O}$ of $\pm 2\%$ (2 SD) (Valley and Graham, 1991) and used as such in several SIMS studies (Hervig et al., 1992; Valley and Graham, 1993; Eiler et al., 1995a,b; Choi et al., 1997, 1998; Riciputi et al., 1998; Choi et al., 2000; Greenwood et al., 2000; Sitzman et al., 2000; Choi and Wasson, 2003; Hsu et al., 2006). A single mm-size crystal from M34572-A was used for oxygen three isotope analyses with a precision of better than $\pm 0.5\%$ (2SD) (Kita et al., 2004) though the grain-to-grain precision of $\delta^{18}\text{O}$ was not strictly evaluated.

Each sample was crushed and the magnetite was separated from the non-magnetic fraction by a hand magnet. Individual 1–2 mg grain fragments (heretofore called grains) were analyzed for $\delta^{18}\text{O}$ by laser fluorination. SIMS mounts were prepared by casting individual 150–300 μm grains of magnetite with UWQ-1, a quartz standard (Kelly et al., 2007), in a 25 mm epoxy round. Five epoxy mounts were made (M3–M7): M3 contains magnetite samples 5830, 5835, and 5847; M4 contains magnetite 08M2; M5 contains magnetite samples 08-BI-12 and M34572-A; M6 contains magnetite samples 5830 and M34572-A; and M7 contains magnetite samples 5830 and LP204-1.

All grains were placed within 5 mm of the center of the epoxy mount to minimize variation in instrumental bias due to X–Y effects (Kita et al., 2009). Sample relief, measured by optical examination, was no more than $\sim 2 \mu\text{m}$. The sample mounts were ground, lapped, cleaned, and then coated with $\sim 20 \text{ nm}$ of carbon for SIMS analysis.

One hematite (Fe_2O_3) sample, 09H1, was analyzed in a similar effort to identify a homogeneous oxygen isotope standard by SIMS. Hematite 09H1 is derived from a coarse-grained quartz–hematite–rutile sample from Brazil with no further information and was obtained from the collections of the UW-Madison Geology Museum. One hematite grain mount was prepared following the same procedure as for magnetite.

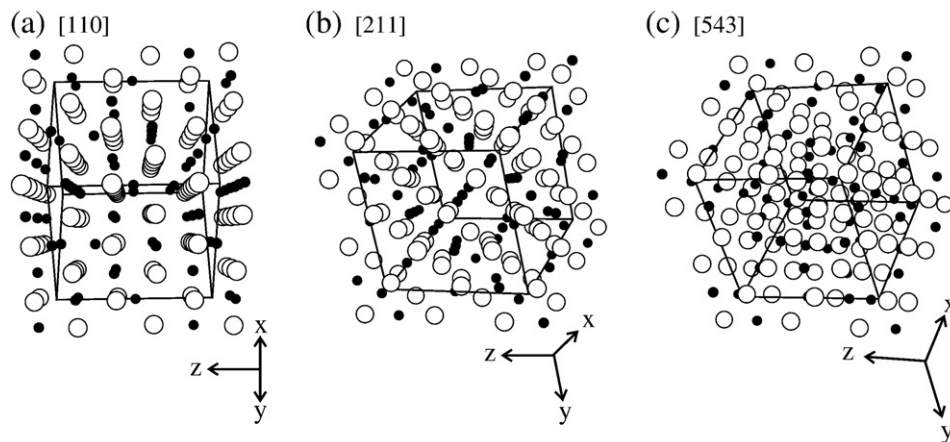


Fig. 2. Perspective renderings of the crystal structure for magnetite using the software CrystalMaker® 8.2. Thin black lines indicate one unit cell (32 oxygens). Iron atoms are shown as black dots, oxygen atoms are open circles, and atomic bonds are not shown. (a) Perspective view looking down [110] and (b) looking down [211] (both views are perpendicular to the page). Oxygen atoms are aligned in rows within planes parallel to the viewing direction. (c) Perspective view looking down the [543] direction, where rows of oxygen atoms are inclined relative to the viewing direction.

3. Experimental procedures

3.1. Laser fluorination

Laser fluorination of 1–2 mg samples was performed at the Stable Isotope Lab, UW-Madison, using BrF₅ reagent and a CO₂ laser ($\lambda = 10.6 \mu\text{m}$) connected to a Finnigan MAT 251 gas-source mass spectrometer. Values of $\delta^{18}\text{O}_{\text{VSMOW}}$ were standardized by comparison with analyses of garnet standard UWG-2, which is calibrated to the quartz standard NBS-28 following procedures described by Valley et al. (1995). The reproducibility of UWG-2 analyses in this study is $\pm 0.1\%$ (2SD).

3.2. EPMA and SEM analysis

Electron probe microanalysis (EPMA) was performed with a CAMECA SX51 electron microprobe at UW-Madison. The operating conditions used were an accelerating voltage of 20 kV, a Faraday cup current of 20 nA, and a tight fixed beam. Natural crystalline standards used were Minas Gerais magnetite USNM 114887 and hematite for Fe, Minas Gerais rutile (TiO₂) for Ti, spinel (MgAl₂O₄) for Mg and Al, and gahnite (ZnAl₂O₄) USNM 145883 for Zn. Synthetic standards used were Mn₂SiO₄ for Mn and Si, vanadium metal for V, and Cr₂O₃ for Cr. Data were reduced using the Probe For EPMA software (Donovan et al., 2010), and the matrix correction utilized was the Armstrong-Love/Scott phi-rho-z method (Armstrong, 1988) modified from Brown and Bastin with Henke Mass Absorption Coefficients. Oxygen was calculated from cation stoichiometry and included in the matrix correction. 50 measurements (5 per grain) were made for magnetites 08M2, 5830, 5835, and 5847; 5 measurements (1 per grain) were made for magnetite 08-BI-12; 20 measurements (1 per grain) were made for magnetite M34572-A; and 23 measurements (1 per grain) were made for hematite 09H1 (Supplemental Table A1). EPMA data for magnetite LP204-1 are reported from Valley and Graham (1991). All analyzed magnetite samples are ≥ 98 wt.% Fe₃O₄ and hematite is ≥ 98 wt.% Fe₂O₃. All reported elements are present above detection limits at 99% confidence levels. Backscatter and secondary electron imaging were performed with a Hitachi S-3400N variable pressure scanning electron microscope (SEM) at UW-Madison.

3.3. SIMS analysis

In situ oxygen isotope analysis (¹⁸O/¹⁶O) was performed using a CAMECA IMS-1280 large radius, multi-collector ion microprobe at the WiscSIMS Laboratory, UW-Madison (Kita et al., 2009; Valley and Kita, 2009). Routine $\delta^{18}\text{O}$ analysis at WiscSIMS utilizes a ¹³³Cs⁺ primary ion beam focused to a diameter of $\sim 10 \mu\text{m}$ with a Gaussian density distribution and a primary beam current of ~ 2.0 nA. The SIMS analysis pits formed by the Gaussian beam have a depth of $\sim 2 \mu\text{m}$ in magnetite, and these analyses are referred to as “deep-pit mode” in this study. The primary and secondary accelerating voltages used were +10 kV and –10 kV respectively, so that the total impact energy is 20 keV. An energy window of 40 eV set at the low energy band (0 to 40 eV) was used for all measurements. Charging of the sample was compensated by the conductivity of a 20 nm carbon coat on the epoxy mount, an electron flood gun, and for magnetite and hematite grains, the natural conductivity of the sample. The total analytical time was ~ 3 min per pit: 20 s presputtering, ~ 1 min automatic centering of the secondary ions in the field aperture, and analysis with 20 cycles of 4 s integration time each. The secondary O[–] ions were simultaneously collected by two Faraday Cup detectors in the multicollector system. The secondary ¹⁶O ion intensity was 3.0×10^9 cps for magnetite and 2.5×10^9 cps for quartz. The secondary ion yield (the ratio of secondary ion intensity and primary beam current) for magnetite varied 7%, from 1.45 – 1.55×10^9 cps/nA, and weakly correlates ($R^2 = 0.2$) with measured $\delta^{18}\text{O}$ values (Supplemental Table A2). The quartz standard, UWQ-1 (Kelly et al., 2007), was analyzed to bracket magnetite and

hematite sample analyses. Four measurements on UWQ-1, with a typical precision of $\pm 0.3\%$ (2SD), were made before and after each group of 10–15 sample measurements in order to monitor the stability of the instrument and correct for internal drift. The seven magnetite samples and one hematite sample were analyzed at the +10 kV/–10 kV condition in deep-pit mode over seven sessions (S1–S7) from August 2008 to September 2009 (Supplemental Table A2).

After analysis, the SIMS pits were examined by SEM for cracks, epoxy, cavities, and mineral inclusions. The depth of the SIMS pits were evaluated by white light profilometer; pits are dish-shaped for analyses made in deep-pit mode. Three magnetite samples (5830, 5835, and 5847) show exsolution lamellae of ilmenite (FeTiO₃), $\sim 0.1 \mu\text{m}$ wide by up to $5.0 \mu\text{m}$ in length, which comprise less than 1% by volume of the sample and thus of the material analyzed from SIMS pits. Magnetite 5847 contains more ilmenite ($\sim 10\%$). When possible, SIMS pits were placed in domains with relatively fewer inclusions. The fractionation in $\delta^{18}\text{O}$ between magnetite and ilmenite is estimated to be less than 0.5‰ at 500 °C (Zheng, 1991). At WiscSIMS, the difference in instrumental bias of $\delta^{18}\text{O}$ between ilmenite and magnetite is not known, though it is unlikely to be larger than 10‰ under routine analytical conditions (Valley and Kita, 2009). Thus the contamination of magnetite by ilmenite was insignificant for these $\delta^{18}\text{O}$ analyses.

The incident angle (θ) of the SIMS primary beam, from normal to the sample surface, is a function of the primary (V_p) and secondary (V_s) accelerating voltages and the primary axis angle (α) of the instrument (CAMECA, 2004):

$$\sin(\theta) = \frac{\sin(\alpha)}{\sqrt{1 - V_s/V_p}} \quad (1)$$

For the CAMECA IMS-1270 and -1280 instruments, the primary axis angle is 30°, and at primary and secondary accelerating voltages of +10 kV and –10 kV respectively, the incident Cs⁺ beam angle is 21° from normal to the sample surface by Eq. (1).

Besides crystal orientation effects, we considered the possibility that a magnetic field locally created by individual magnetite grains may modify the focusing of the electron flood gun used for charge compensation, which could change the instrumental bias. To test this hypothesis, five 150–300 μm grains from three magnetite samples (5830, 5835, and 5847) in M3 were analyzed for $\delta^{18}\text{O}$ by SIMS in deep-pit mode using the conditions described above. A 32 μm thin section was prepared from the same epoxy mount after SIMS analysis, removing most of the mass of each grain but preserving the polished surface. The magnetic field of the magnetite grains was thus reduced. The thin section was remounted in the SIMS sample holder and the same grains were reanalyzed at the same respective crystal orientations as within the epoxy mount.

3.4. SIMS experiments to improve precision in $\delta^{18}\text{O}$

In addition to routine +10 kV/–10 kV analysis in deep-pit mode, four analytical experiments were conducted in attempts to improve the precision in measured $\delta^{18}\text{O}$: (1) applying an energy offset, (2) analyzing in shallow-pit mode, (3) reducing the total impact energy, and (4) varying the primary and secondary accelerating voltages at a constant total impact energy of 13 keV. Magnetite 5830 was analyzed in tests 1–3 on April 1 and 3, 2009, and in test 4 on November 2–5, 2009; hematite 09H1 was analyzed in test 4 on November 5, 2009 (Supplemental Table A3).

3.4.1. Energy offset

In experiment 1, an energy offset of 50 eV was applied (raising the energy window from 0–40 eV to 50–90 eV) by modifying the voltage on the electrostatic analyzer, which resulted in the exclusion of more than 95% of the secondary ions. The Cs⁺ primary ion beam was focused to a

20 μm spot size in deep-pit mode with a primary beam intensity of ~ 1 nA. Total analysis time was 3 min. The secondary O^- ions were collected simultaneously, with the ^{16}O ions by a Faraday Cup detector and the ^{18}O ions by an electron multiplier. The secondary ^{16}O ion intensity was $6\text{--}8 \times 10^7$ cps for magnetite and $4\text{--}5 \times 10^7$ cps for quartz. The secondary ion yield for ^{16}O in magnetite varied by 25% from $0.6\text{--}0.8 \times 10^8$ cps/nA and was $\sim 0.6 \times 10^8$ cps/nA for quartz.

3.4.2. Shallow-pit mode

In experiment 2, the Cs^+ primary ion beam was focused to a diameter of 25 μm with a Köhler illuminated density distribution and a primary beam intensity of ~ 0.2 nA. The SIMS analysis pits formed by the Köhler beam under these conditions, referred to as “shallow-pit mode”, are about 40 times shallower (~ 0.05 μm) in magnetite grains than those formed in deep-pit mode (~ 2 μm). Total analysis time was ~ 6 min: 180 s of presputtering at 0.2 nA, after which the primary beam current was reduced to 60 pA for 20 analysis cycles at 10 s each. The secondary O^- ions were simultaneously collected, with the ^{16}O ions by a Faraday Cup detector and the ^{18}O ions by an electron multiplier. The secondary ^{16}O ion intensity was $4.0\text{--}5.5 \times 10^7$ cps for magnetite and $4.0\text{--}5.0 \times 10^7$ cps for quartz. Secondary ion yields were not calculated due to the low primary beam currents.

3.4.3. Reduced total impact energy

In experiment 3, the primary and secondary accelerating voltages were reduced to +5 kV and -5 kV respectively, so that the total impact energy is 10 keV. The Cs^+ primary ion beam was focused to a diameter of 15 μm in deep-pit mode with a primary beam current of ~ 2.8 nA. Total analysis time was 3 min with the same analytical parameters as used for routine +10 kV/ -10 kV analysis described in Section 3.3. The secondary O^- ions were simultaneously collected by two Faraday Cup detectors in the multicollector system. The secondary ^{16}O ion intensity was $2.0\text{--}2.3 \times 10^9$ cps for magnetite and $1.5\text{--}1.6 \times 10^9$ cps for quartz. The secondary ^{16}O ion yield for magnetite was nearly half of that for analyses made at 20 keV and varied by 12% from $0.7\text{--}0.8 \times 10^9$ cps/nA.

3.4.4. Varying the incident angle of the SIMS primary Cs^+ beam

In experiment 4, three different analytical procedures were conducted to vary the incident angle of the SIMS primary Cs^+ beam at a constant total impact energy. Primary/secondary accelerating voltages of +10 kV/ -3 kV, +6.5 kV/ -6.5 kV, and +3 kV/ -10 kV (total impact energy 13 keV) were used, resulting in incident angles (θ) of 26° , 21° , and 14° respectively of the Cs^+ beam from normal to the sample surface. All analyses were made with a Köhler illuminated primary beam although the analysis pits are dish-shaped (as in deep-pit mode) as determined by white light profilometer. The secondary O^- ions were simultaneously collected by two Faraday Cup detectors in the multicollector system. The total analytical time for individual analyses in each procedure was ~ 3 min with the same analytical parameters as used for routine +10 kV/ -10 kV analysis described in Section 3.3.

For +10 kV/ -3 kV analysis, a Cs^+ primary ion beam was focused to a 20×25 μm spot size with a primary beam current of ~ 3.5 nA. This relatively high beam current was used to increase the total secondary ion counts due to the low secondary accelerating voltage. The secondary ^{16}O ion intensity was $0.6\text{--}0.8 \times 10^9$ cps for magnetite and $0.6\text{--}0.7 \times 10^9$ cps for quartz. The secondary ^{16}O ion yield varied significantly, by 40% from $0.15\text{--}0.25 \times 10^9$ cps/nA for magnetite and was $\sim 0.2 \times 10^9$ cps/nA for quartz.

For +6.5 kV/ -6.5 kV analysis, a Cs^+ primary ion beam was focused to a 18×25 μm spot size with a primary beam current of 1.4 nA. The secondary ^{16}O ion intensity was $1.0\text{--}1.2 \times 10^9$ cps for magnetite and $0.9\text{--}1.0 \times 10^9$ cps for quartz. The secondary ^{16}O ion yield varied by 11% from $0.8\text{--}0.9 \times 10^9$ cps/nA for magnetite and was $0.6\text{--}0.7 \times 10^9$ cps/nA for quartz.

For +3 kV/ -10 kV analysis, a Cs^+ primary ion beam was focused to a 15×30 μm spot size. In the first session, the primary beam current was 1.4 nA. The secondary ^{16}O ion intensity was $1.7\text{--}1.8 \times 10^9$ cps for magnetite and $\sim 1.3 \times 10^9$ cps for quartz. The secondary ^{16}O ion yield varied by 8% from $1.2\text{--}1.3 \times 10^9$ cps/nA for magnetite and was $\sim 1.0 \times 10^9$ cps/nA for quartz. In the second session, the primary beam current was 1.15 nA. The secondary ^{16}O ion intensity was $1.5\text{--}1.6 \times 10^9$ cps for magnetite and $\sim 1.2 \times 10^9$ cps for quartz. The secondary ^{16}O ion yield varied by 7% from $1.3\text{--}1.4 \times 10^9$ cps/nA for magnetite and was $\sim 1.0 \times 10^9$ cps/nA for quartz.

3.5. EBSD analysis

Electron backscatter diffraction (EBSD) was used to determine the crystal orientation of magnetite grains in epoxy mounts. The magnetite grains used in this study are crushed grain fragments and do not show euhedral crystal faces or parting and thus were distributed in random orientations. Sample mounts were polished for ~ 1 h with a 0.05 μm colloidal silica polishing suspension to remove surface damage created by mechanical polishing and then analyzed uncoated in variable pressure mode in the SEM. EBSD measurements were made with an Oxford Instruments NordlysS detector and an accelerating voltage of 20 kV on a Hitachi S-3400 N SEM at the UW-Madison. Electron backscatter patterns (EBSPs) were collected on a phosphor screen, and processed using the Oxford Instruments software package CHANNEL5 in point collection mode. Six to twelve EBSPs were acquired for each grain. Each EBSP has a mean angular deviation (MAD: a measure of the residuals of the simulated EBSP match to the actual EBSP) of less than 1° . Euler angles ($z\text{--}x\text{--}z$ notation) from the EBSP with the lowest MAD are used to determine the crystal orientation for each magnetite grain.

To increase the accuracy of comparing crystal orientations by EBSD and SIMS data, we marked azimuths of 000° , 090° , 180° , and 270° on the sample holders for both instruments and on the back of each grain mount and defined the North position. Thus, a mount can be placed at a specific orientation in the EBSD holder and the same orientation can be reproduced at $\pm 2^\circ$ in the SIMS holder and vice versa. In session 7, the sample mounts were reoriented in the SIMS holder by measuring the X–Y coordinates for SIMS analysis pits from the previous session and rotating the mount in the sample holder until it was placed within $\pm 1^\circ$ of its previous orientation.

3.6. Stereographic projection

The high symmetry of the magnetite crystal structure (face-centered cubic, m3m) allows a lower hemisphere stereographic projection to be divided into 24 symmetrically equivalent regions (called cubic standard triangles) with corners at $\langle 100 \rangle$, $\langle 111 \rangle$, and $\langle 110 \rangle$. Thus, magnetite crystal orientations are plotted within a single cubic standard triangle at $[110]$, $[111]$, and $[110]$ for the purposes of this study.

In order to correlate the SIMS and EBSD data, measured $\delta^{18}\text{O}$ values were assigned to the incident Cs^+ beam directions for individual grains. For routine +10 kV/ -10 kV analysis, the Cs^+ beam incident angle is calculated to be 21° from normal to the sample surface using Eq. (1), and the Cs^+ beam direction is thus plotted for individual grains of magnetite. Angles between $[110]$, $[111]$, and $[110]$ and the Cs^+ beam direction were measured, then replotted on a $[111]$ -centered equal area lower hemisphere stereographic projection within the cubic standard triangle using the software Stereo32 (Röller and Trepmann, 2008). Measured $\delta^{18}\text{O}$ values were contoured using block kriging and radial basis function gridding methods using the software 3DFieldPro (Galouchko, 2008).

There are several sources of uncertainty in the estimation of crystal orientation of magnetite grains in epoxy mounts. The reproducibility in manual placement of the sample at the same azimuth in SIMS and EBSD sample holders is visually estimated to be $\pm 2^\circ$. The uncertainty

in the fitting of the Kikuchi pattern, the mean angular deviation (MAD), is always better than $\pm 1^\circ$ and in general, less than $\pm 0.5^\circ$ for all EBSD patterns reported in this study. Multiple EBSD measurements were made on each grain and misorientations within individual grains are less than $\pm 2^\circ$. Replotting of Cs^+ beam directions in the [111]-centered projection has an uncertainty of $\pm 1^\circ$. Thus, the cumulative uncertainty in the stereographic projection of the Cs^+ beam direction for individual magnetite grains is estimated to be $\pm 4^\circ$.

4. Results

4.1. SIMS analyses of $\delta^{18}\text{O}$ in magnetite

Fig. 3 shows raw measured values of $\delta^{18}\text{O}$ without correction for bias or instrumental drift ($\delta^{18}\text{O}_{\text{Raw}}$) for the quartz (Qt) standard

UWQ-1 and magnetite (Mt) 5830 for +10 kV/–10 kV analysis in deep-pit mode. In Fig. 3a, measured values of $\delta^{18}\text{O}(\text{Qt})_{\text{Raw}}$ (squares) have an average precision of $\pm 0.3\%$ (2SD) in bracketing groups of eight to ten analyses. In this study, precision is always reported as 2SD for n analyzed grains. Spot-to-spot reproducibility for quartz is the same in single grains and from grain-to-grain. In contrast, measured values of $\delta^{18}\text{O}(\text{Mt})_{\text{Raw}}$ (circles) have an average precision of $\pm 2.1\%$ ($n = 188$) from grain-to-grain of magnetite. In Fig. 3b, the average grain-to-grain precision for magnetite is $\pm 2.9\%$ ($n = 26$), reflecting fewer total analyses and the selection of grains with extreme values to bracket the range in measured $\delta^{18}\text{O}$, while the average precision in single grains of magnetite analyzed three or more times is $\pm 0.4\%$ ($n = 12$), close to $\pm 0.3\%$, that obtained for the homogeneous quartz standard. Relatively poor reproducibility as high as $\pm 0.9\%$ within some magnetite

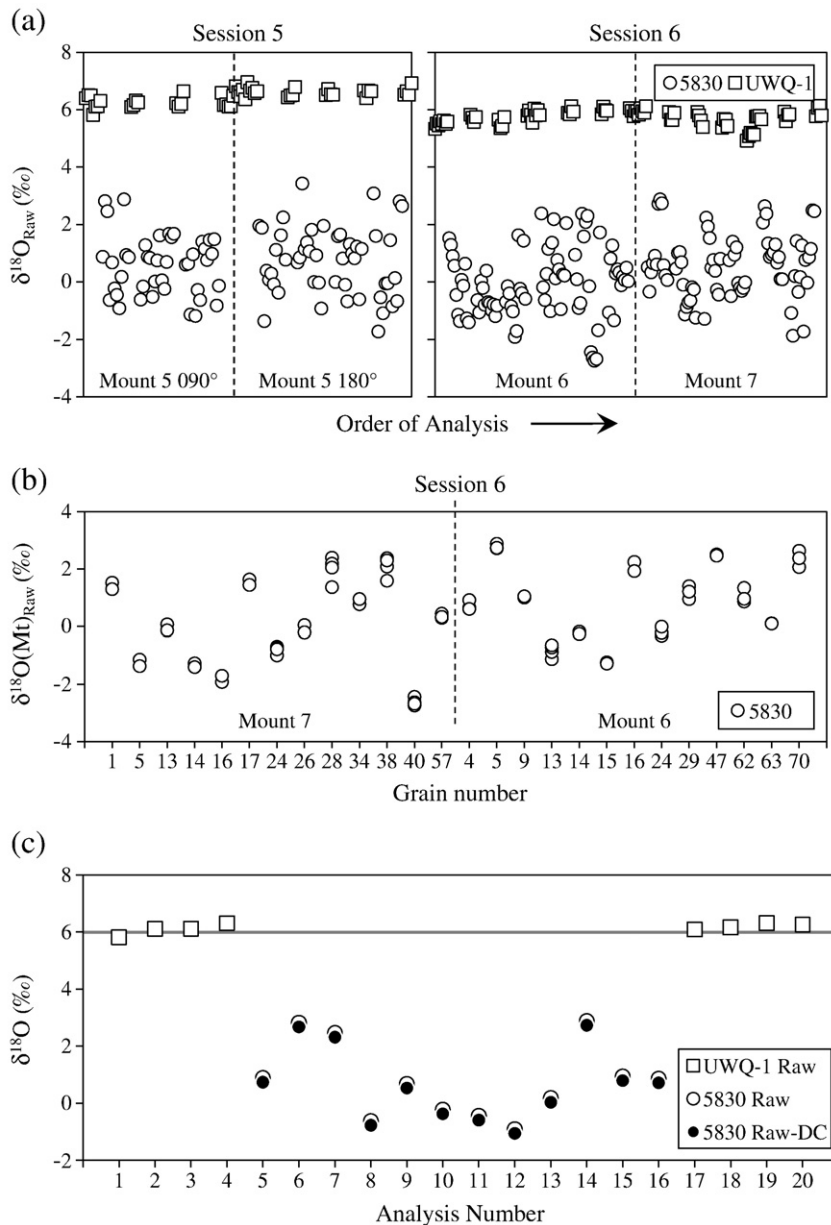


Fig. 3. (a) Values of $\delta^{18}\text{O}_{\text{Raw}}$, the raw measured SIMS value without correction for drift or instrumental bias, for magnetite 5830 and the quartz standard UWQ-1. Each group of 10–15 analyses of magnetite (circles) are bracketed by 8 analyses of UWQ-1 (squares). The average precision for each group of 8 quartz analyses is $\pm 0.3\%$ (2SD), both in single grains and from grain-to-grain. In contrast, the average grain-to-grain precision for magnetite is $\pm 2.1\%$ (2SD, $n = 188$). Dashed lines indicate sample changes. (b) Multiple analyses of $\delta^{18}\text{O}(\text{Mt})_{\text{Raw}}$ in single grains of magnetite 5830. The grain-to-grain precision for magnetite is $\pm 2.9\%$ (2SD, $n = 26$), while the average precision in single grains analyzed three or more times is $\pm 0.4\%$ (2SD, $n = 12$). Dashed line indicates sample change. (c) An example of drift correction for one bracket. The precision of measured $\delta^{18}\text{O}$ values for magnetite is not improved by correcting for instrumental drift.

grains likely reflects heterogeneity documented at the mm-scale by laser fluorination.

Accurate SIMS analysis requires comparison to a standard of the same chemical composition and crystal structure as the sample. Therefore, instrumental bias is calibrated using well-characterized homogeneous isotope mineral standards (Kita et al., 2009; Valley and Kita, 2009). In this study, instrumental bias in $\delta^{18}\text{O}$ for the quartz standard UWQ-1 changes by 0.5–1.0‰ within an individual SIMS session and by up to 2‰ from one session to another (over a 16 month period) due to slight differences in instrumental conditions. Magnetite sample analyses, $\delta^{18}\text{O}(\text{Mt})_{\text{Raw}}$, obtained in different sessions are bracketed by analyses of UWQ-1, $\delta^{18}\text{O}(\text{Qt})_{\text{Raw}}$, thus providing a basis for drift correction of bracketed sample analyses. The drift corrected values of $\delta^{18}\text{O}$ for magnetite, $\delta^{18}\text{O}(\text{Mt})_{\text{Raw-DC}}$, are normalized to $\delta^{18}\text{O}(\text{UWQ-1})_{\text{Raw-DC}} = 6.0\text{‰}$, and an example is shown for one bracket (Fig. 3c). The true value for UWQ-1 is 12.33‰ VSMOW, and 6.0‰ is the typical raw measured value, reflecting the average instrumental bias for quartz analyses (−6.33‰) over the SIMS sessions reported here. Values of $\delta^{18}\text{O}(\text{Mt})_{\text{Raw-DC}}$ are not corrected to the VSMOW scale and are used for comparative purposes only. In Fig. 3, the precision for measured $\delta^{18}\text{O}$ values of magnetite 5830 is not improved by correcting for instrumental drift using bracketing $\delta^{18}\text{O}$ values of UWQ-1.

Values of $\delta^{18}\text{O}(\text{Mt})_{\text{Raw-DC}}$ for magnetites 5830 and M34572-A analyzed over nine months in six SIMS sessions (S1–S6) are shown in Supplemental Fig. A1. Precision in measured $\delta^{18}\text{O}$ is poor but consistent in each session, ± 2.0 – 2.2‰ for magnetite 5830 (circles), and ± 1.8 – 2.2‰ for magnetite M34572-A (diamonds). However, the average values for $\delta^{18}\text{O}(\text{Mt})_{\text{Raw-DC}}$ in both magnetite samples change by +1.5‰ between S3 and S4, suggesting that bias changed due to differences in instrumental conditions. Thus, only data from sessions with the same average bias (S1–S3 and S4–S6) are combined for

calculating average $\delta^{18}\text{O}_{\text{Raw-DC}}$ values of magnetites 5830 and M34572-A.

All seven magnetite samples were analyzed for $\delta^{18}\text{O}$ by laser fluorination (Supplemental Table A4). Precision by laser for single 2 mg chips of five magnetite samples is ± 0.1 – 0.3‰ (2SD, $n = 5$), $\pm 0.5\text{‰}$ for 08-BI-12, and $\pm 0.7\text{‰}$ for M34572-A, reflecting mm-scale heterogeneity. The grain-to-grain precision by SIMS is significantly worse but remarkably consistent, ± 2 – 3‰ (2SD, $n \geq 10$), for all seven samples (Supplemental Table A5). Average values of $\delta^{18}\text{O}(\text{Mt})_{\text{Raw-DC}}$, the drift-corrected measured SIMS value, are plotted against $\delta^{18}\text{O}(\text{Mt})_{\text{VSMOW}}$, the calibrated value by laser fluorination, for all seven magnetite samples in Supplemental Fig. A2. Magnetites 5830 and M34572-A are plotted twice, separated into sessions with the same average bias. Dashed lines for $\Delta^{18}\text{O}$ (SIMS-Laser) = −3 and −6‰ bound the average bias for all magnetite samples in this study.

4.1.1. Effect of magnetism from magnetite grains on $\delta^{18}\text{O}$

The magnetism of magnetite sample grains was evaluated as a possible cause of variation in measured $\delta^{18}\text{O}$. Three magnetite samples, 5830, 5835, and 5847, were analyzed in a 32 μm thick petrographic thin section and in an epoxy mount (M3). The same five grains were analyzed at the same respective crystal orientations in both the thin section and epoxy mount. Values of $\delta^{18}\text{O}(\text{Mt})_{\text{Raw}}$ in the epoxy mount and thin section have an average residual of 0.5‰ to a 1:1 line (Supplemental Fig. A3). The offset in $\delta^{18}\text{O}(\text{Mt})_{\text{Raw}}$ values between the thin section and epoxy mount is due to the difference in instrumental bias between the two sessions and is not significant. The average range in measured $\delta^{18}\text{O}(\text{Mt})_{\text{Raw}}$ values is $\sim 5\text{‰}$ for the five magnetite grains in each sample, and measured $\delta^{18}\text{O}$ values are reproducible for individual magnetite grains. In other studies, no difference is seen in the precision and range in measured $\delta^{18}\text{O}$ values for magnetite from matching 32 μm

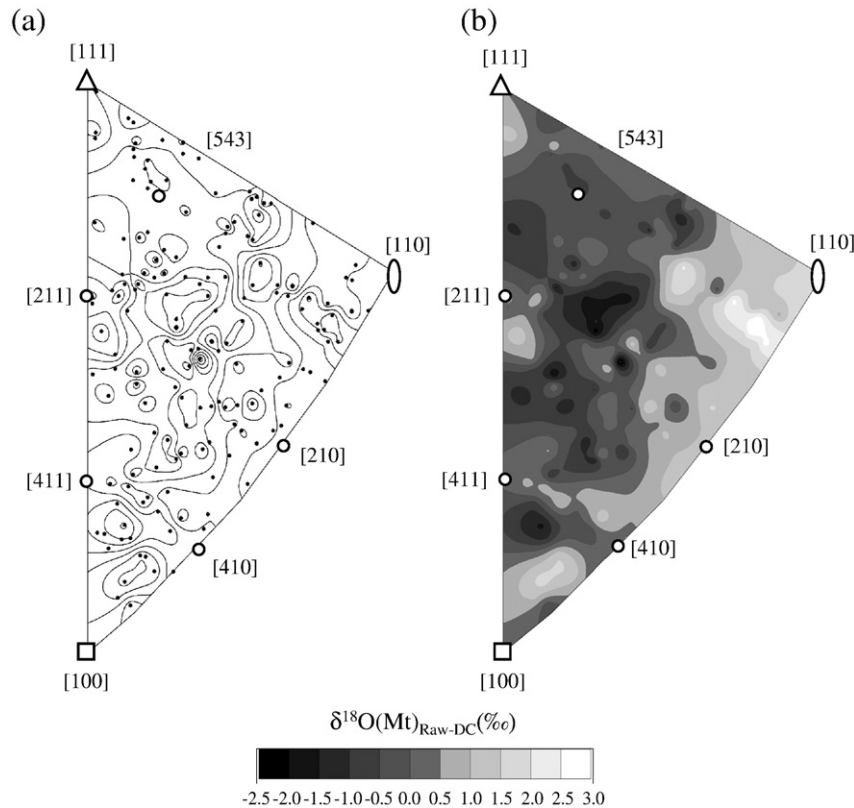


Fig. 4. Cubic standard triangle contoured for values of $\delta^{18}\text{O}(\text{Mt})_{\text{Raw-DC}}$ for magnetite 5830. The directions [110], [100], and [111] define the cubic standard triangle for magnetite and other cubic crystals. (a) The stereographic projection of the incident Cs^+ beam direction is plotted for individual magnetite grains (black dots) and 0.5‰ contours of $\delta^{18}\text{O}$ are derived from Block Kriging (Galouchko, 2008). (b) Shaded contours showing correlation between high $\delta^{18}\text{O}(\text{Mt})_{\text{Raw-DC}}$ values (light shades of grey, $\delta^{18}\text{O}(\text{Mt})_{\text{Raw-DC}} \geq 0.5\text{‰}$) and $\langle u|v \rangle$, from [110] to [100] and from [211] to [210] and [411] to [410].

thin sections and mm-thick rock chips mounted in epoxy. The possibility of magnetic effects was also evaluated by observing the image of the low energy electron cloud on the sample as the electron beam was placed directly on magnetite, hematite, quartz, and epoxy. No deflection in the shape or intensity of the electron cloud was observed. Thus, the magnetism of magnetite grains is not supported as the cause of variation in $\delta^{18}\text{O}$ for these analyses.

4.2. Correlation of SIMS and EBSD analyses

To evaluate differences in crystal orientation of magnetite grains as a possible cause of variation in measured $\delta^{18}\text{O}$, we made SIMS analyses and EBSD measurements on 155 grains of magnetites 5830 and M34572-A at 193 different crystal orientations (Supplemental Tables A2 and A6). The incident Cs^+ beam direction was plotted relative to the magnetite crystal structure on a [111]-centered cubic standard triangle. Values of $\delta^{18}\text{O}_{\text{Raw-DC}}$ were assigned to the Cs^+ beam directions for individual grains, and the area between [111], [110], and [100] was contoured for $\delta^{18}\text{O}$. The average $\delta^{18}\text{O}_{\text{Raw-DC}}$ value was used for multiple analyses within single grains.

Fig. 4 shows results for magnetite 5830. In this and subsequent projections, we show only the smallest symmetrically unique area, the cubic standard triangle. Actual SIMS analyses were made with the position of the Cs^+ beam fixed and with varying crystal orientations for randomly mounted magnetite grains. For simplicity, the Cs^+ beam directions are plotted in a common reference frame on a [111]-centered cubic standard triangle, as if individual grains were in the same orientation and the Cs^+ beam was moved. More than one orientation for individual grains was measured for grains analyzed at different orientations (azimuths) of the sample holder. EBSD and SIMS data were collected from 159 different orientations of 121 grains in

three mounts (M3, M6, and M7) during two SIMS sessions (S5 and S6). M3 was analyzed at azimuths of 090° and 180° , and M6 and M7 at 000° .

Fig. 4a shows the stereographic projection of the Cs^+ beam direction for individual grains of magnetite 5830 (black dots, $n = 159$) and contours of $\delta^{18}\text{O}$ at 0.5‰ intervals. Fig. 4b shows the same projection with contoured domains shaded in grey scale. High $\delta^{18}\text{O}$ values (light shades of grey, $\delta^{18}\text{O}(\text{Mt})_{\text{Raw-DC}} \geq 0.5\text{‰}$) are measured when the Cs^+ beam is parallel to the set of directions $\langle uv0 \rangle$, from [110] to [100]. The highest $\delta^{18}\text{O}$ values are found close to [110]. Values of $\delta^{18}\text{O}$ decrease along $\langle uv0 \rangle$, from [110] to [100], and the field of high $\delta^{18}\text{O}$ values extends 12° from [110] and narrows to within 7° at [100]. In addition, high $\delta^{18}\text{O}$ values are measured from [211] to [210] and from [411] to [410].

Fig. 5 shows results for magnetite M34572-A. Data were collected from 34 grains (one orientation per grain) in two mounts (M5 and M6) during two SIMS sessions (S5 and S6). M5 was analyzed at 090° and M6 at 000° . Fig. 5a shows the stereographic projection of the Cs^+ beam direction for individual grains of magnetite M34572-A (black dots, $n = 34$) and contours of $\delta^{18}\text{O}$ at 0.5‰ intervals. Fig. 5b shows the same projection with contoured domains shaded in grey-scale. High $\delta^{18}\text{O}$ values (light shades of grey, $\delta^{18}\text{O}(\text{Mt})_{\text{Raw-DC}} \geq -4\text{‰}$) are measured when the Cs^+ beam is parallel to $\langle uv0 \rangle$, from [110] to [100], and the same trends are seen as for magnetite 5830 in Fig. 4b. Details of the contours between the two magnetite samples differ largely due to the fewer number of data points for magnetite M34572-A (Fig. 5, $n = 34$) than for magnetite 5830 (Fig. 4, $n = 159$).

During SIMS analysis, magnetite grains with extreme $\delta^{18}\text{O}$ values were chosen to ensure the full range in $\delta^{18}\text{O}$ was measured in a single session. Multiple analyses were made to obtain precise $\delta^{18}\text{O}$ values for these grains. High $\delta^{18}\text{O}$ values were also preferentially analyzed for

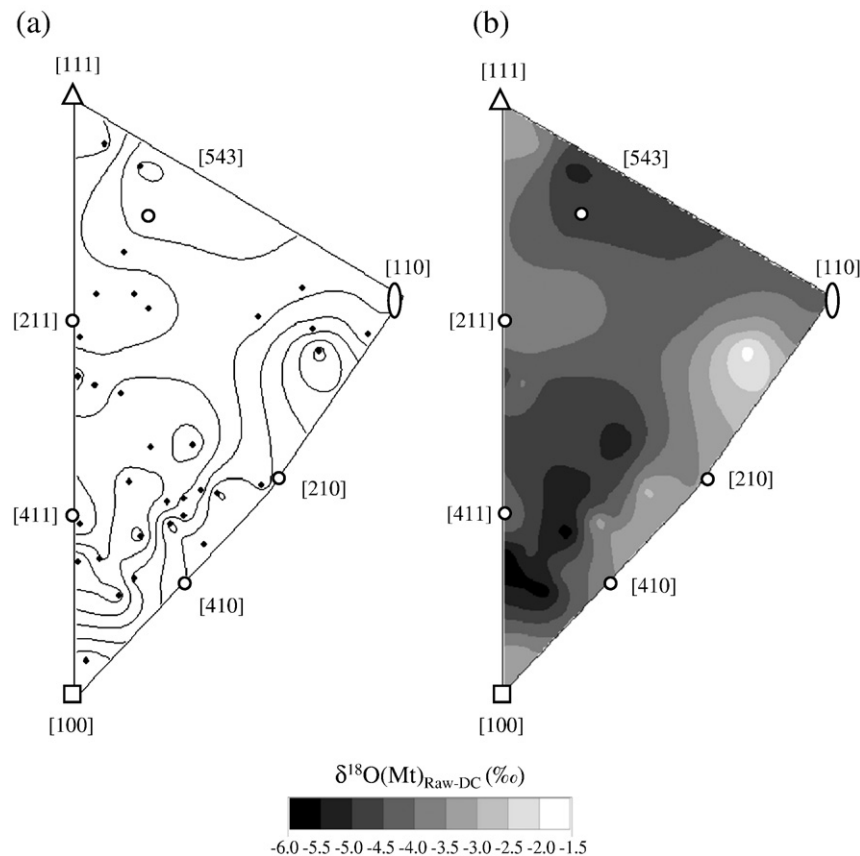


Fig. 5. Cubic standard triangle contoured for values of $\delta^{18}\text{O}(\text{Mt})_{\text{Raw-DC}}$ for magnetite M34572-A. (a) The stereographic projection of the incident Cs^+ beam direction for individual magnetite grains (black diamonds) and 0.5‰ contours of $\delta^{18}\text{O}$ are derived from Block Kriging (Galouchko, 2008). (b) Shaded contours show the correlation between high $\delta^{18}\text{O}$ ($\text{Mt})_{\text{Raw}}$ values (light shades of grey, $\delta^{18}\text{O}(\text{Mt})_{\text{Raw-DC}} \geq -4\text{‰}$) and $\langle uv0 \rangle$, from [110] to [100].

grains oriented with the Cs^+ beam parallel to $\langle uv0 \rangle$. The average precision in measured $\delta^{18}\text{O}$ of $\pm 2\text{--}3\%$ (2SD) likely would be smaller for a perfectly random data set. To evaluate this possibility, Image J (NIH) software (Rasband, 2010) was used to calculate $\delta^{18}\text{O}$ values based on the areal distribution of grey scale values (0.5% domains) in the contoured standard triangles.

Fig. 6 shows histograms of average $\delta^{18}\text{O}(\text{Mt})_{\text{Raw-DC}}$ values measured by SIMS (black bars) and calculated from the grey scale values (white bars) in Figs. 4b and 5b normalized to the number of SIMS analyses for magnetite samples 5830 and M34572-A respectively. The average $\delta^{18}\text{O}(\text{Mt})_{\text{Raw-DC}}$ value by SIMS is identical to the average $\delta^{18}\text{O}$ values calculated from the grey scale values, indicating that the selected gridding methods do not bias the mean value for the data. The calculated precision in measured $\delta^{18}\text{O}$ from the grey scale values in the contoured standard triangles is $\pm 1.5\%$ (2SD), suggesting that the precision for a data set with perfectly distributed random orientations would be better than was measured for these magnetite analyses.

4.3. Analytical experiments to improve precision in $\delta^{18}\text{O}$

Four analytical experiments were conducted to improve precision in measured $\delta^{18}\text{O}$ for magnetite by SIMS. As previously, specific crystal

orientations of magnetite grains were preferentially analyzed to obtain extreme $\delta^{18}\text{O}$ values and bracket the range in measured $\delta^{18}\text{O}$. Thus for these grains, values of $\delta^{18}\text{O}_{\text{Raw-DC}}$ have a worse grain-to-grain precision, $\pm 2.5\text{--}3.3\%$ (2SD) than $\pm 2.1\%$, that obtained for 159 orientations of magnetite 5830 which approaches a random distribution.

4.3.1. Experiment 1: energy offset analyses

In experiment 1, we applied an additional 50 eV energy offset, raising the energy window from 0–40 eV to 50–90 eV by modifying the voltage on the electrostatic analyzer which excluded more than 95% of the secondary ions. The pit depths are 1.0–1.2 μm , measured by white light profilometer. Previous studies have shown that high energy offsets can improve the precision of stable isotope analyses in SIMS instruments using a single electron multiplier detector (Hervig et al., 1992; Riciputi et al., 1998; Valley et al., 1998) though the analytical precision for these studies is $\pm 2\%$ (2SD). Fig. 7a shows results of magnetite analyses with normal energy offset (X-axis) compared with results using an additional 50 eV offset (Y-axis). Precision in measured $\delta^{18}\text{O}$ for these analyses shows no significant difference, $\pm 2.9\%$ and $\pm 3.1\%$ (2SD, $n = 19$) respectively. There is no correlation ($R^2 = 0.01$) for a linear fit to the data and large residuals ($X = 9.6$, $Y = 1.6$). Clearly, this experiment was not successful in improving precision in measured $\delta^{18}\text{O}$.

4.3.2. Experiment 2: shallow-pit mode analyses

In experiment 2, the primary Cs^+ ion beam was changed from a Gaussian beam density distribution (deep-pit mode) focused to a 10 μm diameter spot size to a Köhler illuminated primary beam (shallow-pit mode) focused to a 25 μm diameter spot size. The pit depths are 30–50 nm, measured by white light profilometer, ~ 40 times shallower than those made in deep-pit mode. Secondary ^{16}O ion count rates are lower for magnetite analyses made in shallow-pit mode compared to deep-pit mode because of the lower primary beam intensity used. Results from experiment 2 are shown in Fig. 7b. Precision in measured $\delta^{18}\text{O}$ is $\pm 3.3\%$ and $\pm 2.9\%$ (2SD, $n = 11$) for magnetite analyses made in deep-pit mode (X-axis) and shallow-pit mode (Y-axis) respectively. The slope of a linear fit to the data is 0.44, and there is a weak correlation ($R^2 = 0.26$) and large residuals ($X = 7.0$, $Y = 1.0$). Thus shallow-pit mode analysis had limited success in improving precision in measured $\delta^{18}\text{O}$.

4.3.3. Experiment 3: reduced total impact energy analyses

In experiment 3, the primary and secondary accelerating voltages were reduced to +5 kV and -5 kV respectively so that the total impact energy was 10 keV. The pit depths are 0.5–0.6 μm , measured by white light profilometer. Fig. 7c plots magnetite analyses with total impact energies of 20 keV (X-axis) and 10 keV (Y-axis). Precision in measured $\delta^{18}\text{O}$ for magnetite is $\pm 3.3\%$ and $\pm 1.9\%$ (2SD, $n = 11$) respectively. Precision for the quartz standard is worse at 10 keV ($\pm 0.6\%$) than at 20 keV ($\pm 0.3\%$) because of the reduced peak-to-background ratio for secondary ^{18}O counts. The slope of a linear fit to the data is 0.29, there is a weak correlation ($R^2 = 0.26$), and the average residual is the lowest among tests 1–3 ($X = 2.2$, $Y = 0.6$). The results of this experiment show that precision in measured $\delta^{18}\text{O}$ is improved by reducing the total impact energy.

4.3.4. Experiment 4: analyses at varying incident Cs^+ beam angles

In experiment 4, the primary and secondary accelerating voltages were modified in order to vary the incident Cs^+ beam angle at a constant total impact energy of 13 keV. Primary/secondary accelerating voltages of +10 kV/ -3 kV, +6.5 kV/ -6.5 kV, and +3 kV/ -10 kV were used, resulting in calculated incident Cs^+ beam angles (θ) of 26°, 21°, and 14° respectively from normal to the sample surface. The incident Cs^+ beam angle for routine +10 kV/ -10 kV analysis is 21°.

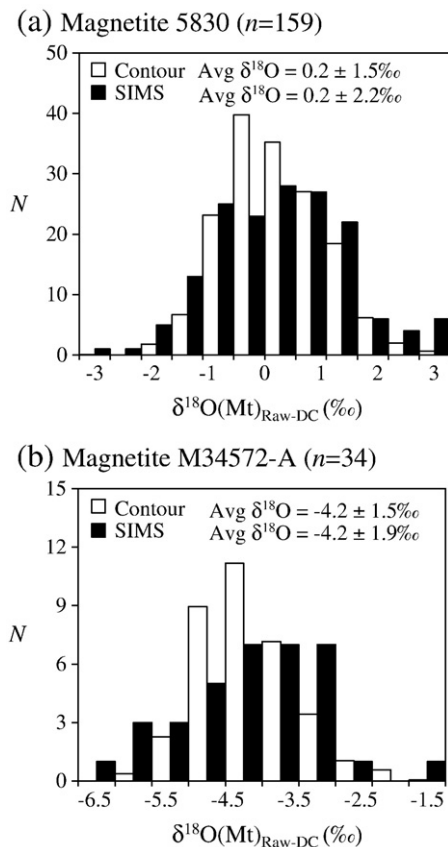


Fig. 6. Histograms of $\delta^{18}\text{O}(\text{Mt})_{\text{Raw-DC}}$ values. Image processing software NIH ImageJ (Rasband, 2010) was used to analyze the distribution of grey scale values in the contoured standard triangles (Figs. 4b and 5b). (a) Magnetite 5830. (b) Magnetite M34572-A. Average values of $\delta^{18}\text{O}$ by SIMS are in excellent agreement with the average $\delta^{18}\text{O}$ value calculated from the grey scale values in the contoured standard triangles normalized to the number of SIMS analyses for each sample. Thus the contouring method does not bias the mean value of the data. The calculated precision in measured $\delta^{18}\text{O}$ from the grey scale values in the contoured standard triangles is $\pm 1.5\%$, suggesting that the precision for a data set with perfectly distributed random orientations would be better than was measured for these magnetite analyses.

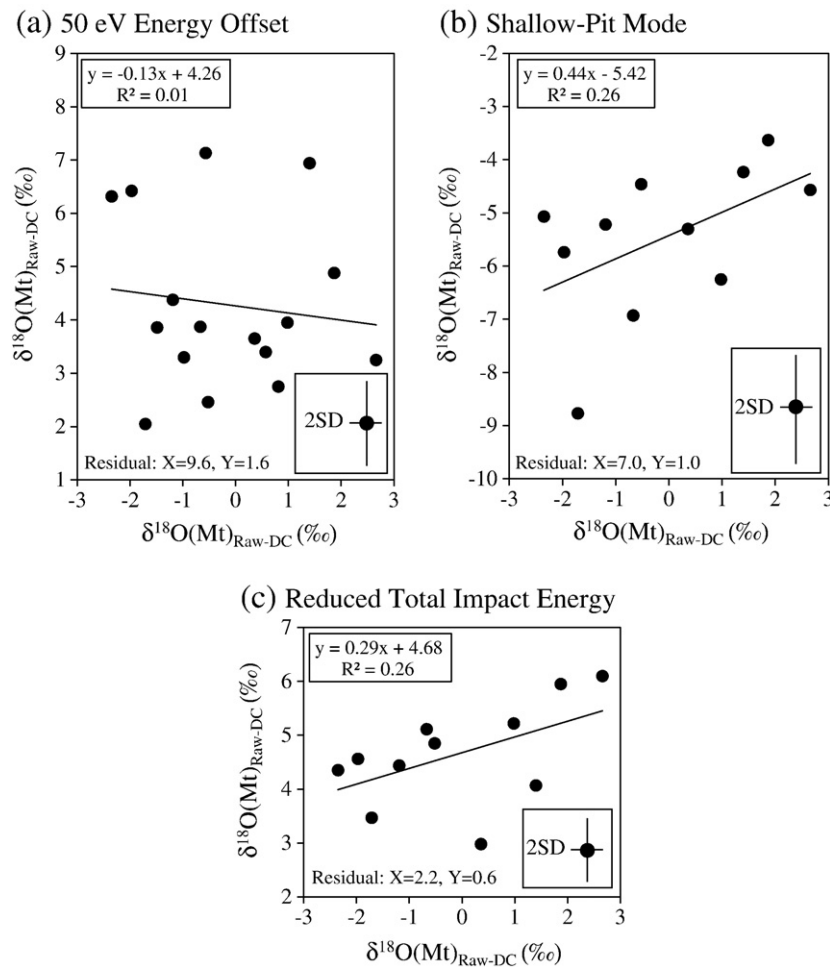


Fig. 7. Results of experiments 1–3 intended to improve precision in measured $\delta^{18}\text{O}$ for magnetite. 2SD is shown for bracketing UWQ-1 quartz standard analyses at the respective analytical procedures. 11 to 19 grains of magnetite 5830 with different crystal orientations have a grain-to-grain precision of $\pm 2.9\%$ to $\pm 3.3\%$ (2SD) (X-axes, Fig. 7a–c). (a) With an additional energy offset of 50 keV (X to Y axes), the grain-to-grain precision did not change appreciably, from $\pm 2.9\%$ to $\pm 3.1\%$ (2SD, $n = 19$). (b) A Köhler illuminated primary beam (shallow-pit mode) was used, and the grain-to-grain precision improved slightly, from $\pm 3.3\%$ to $\pm 2.9\%$ (2SD, $n = 11$). (c) The primary and secondary voltages were modified to +5 kV and –5 kV respectively, and the grain-to-grain precision improved from $\pm 3.3\%$ to $\pm 1.9\%$ (2SD, $n = 11$).

Fig. 8a shows results of magnetite analyses with primary/secondary voltages at +10 kV/–10 kV (X-axis) and +10 kV/–3 kV (Y-axis). The pit depths are 1.4 μm , measured by white light profilometer. Precision in measured $\delta^{18}\text{O}$ is $\pm 2.5\%$ and $\pm 2.2\%$ (2SD, $n = 13$) for +10 kV/–10 kV and +10 kV/–3 kV analysis respectively. The slope of a linear fit to the data is 0.28, and there is a very weak correlation ($R^2 = 0.10$) and large residuals ($X = 3.0, Y = 2.1$). There are some limitations based on instrument geometry, and it is difficult to align the electron flood gun so that the primary Cs^+ beam is homogeneously surrounded by the electric field. This caused an instability of the secondary ion intensity (unstable signal). The precision for brackets of eight quartz analyses is significantly degraded ($\pm 1\%$) for this experiment compared to +10 kV/–10 kV analysis in deep-pit mode ($\pm 0.3\%$). Thus, this experiment was not successful in improving precision in measured $\delta^{18}\text{O}$.

Fig. 8b shows results of magnetite analyses at +10 kV/–10 kV (X-axis) and +6.5 kV/–6.5 kV (Y-axis). The pit depths are 0.6 μm , measured by white light profilometer. Precision in measured $\delta^{18}\text{O}$ improves from $\pm 2.9\%$ to $\pm 1.8\%$ (2SD, $n = 26$) for +10 kV/–10 kV and +6.5 kV/–6.5 kV analysis respectively. The slope of a linear fit to the data is 0.32, and there is a weak correlation ($R^2 = 0.27$) and large residuals ($X = 1.8, Y = 2.1$). As in experiment 3 (+5 kV/–5 kV

analysis), when the total impact energy is reduced at the same incident Cs^+ beam angle, precision in measured $\delta^{18}\text{O}$ is improved.

Fig. 8c shows results of magnetite analyses at +10 kV/–10 kV (X-axis) and +3 kV/–10 kV (Y-axis). Pit depths are 0.4 μm , measured by white light profilometer. The +3 kV/–10 kV analytical procedure was used in two sessions, and the same magnetite grains were analyzed at the same respective crystal orientations in each session as were previously analyzed at +10 kV/–10 kV in deep-pit mode. Precision in measured $\delta^{18}\text{O}$ for magnetite improves from $\pm 2.9\%$ to $\pm 0.8\%$ (2SD, $n = 26$) for +10 kV/–10 kV and +3 kV/–10 kV analysis respectively, while precision for quartz analyses is $\pm 0.3\%$ in both. The slopes of linear fits to the data are 0.11 and 0.14, and residuals are the lowest among all of the analytical experiments ($X = 1.7$ and $2.4, Y = 0.2$ and 0.3). Thus, the +3 kV/–10 kV analytical procedure was the most successful in improving precision in measured $\delta^{18}\text{O}$.

Fig. 8d shows results of magnetite analyses at +3 kV/–10 kV from the 1st session (X-axis) and 2nd session (Y-axis). Residuals to a X=Y line (0.2%) are within analytical precision (2SD) for bracketing analyses of the quartz standard ($\pm 0.3\%$). Fig. 8e shows the results of multiple analyses in single grains of magnetite for +3 kV/–10 kV analysis. The average precision in measured $\delta^{18}\text{O}$ in single grains of

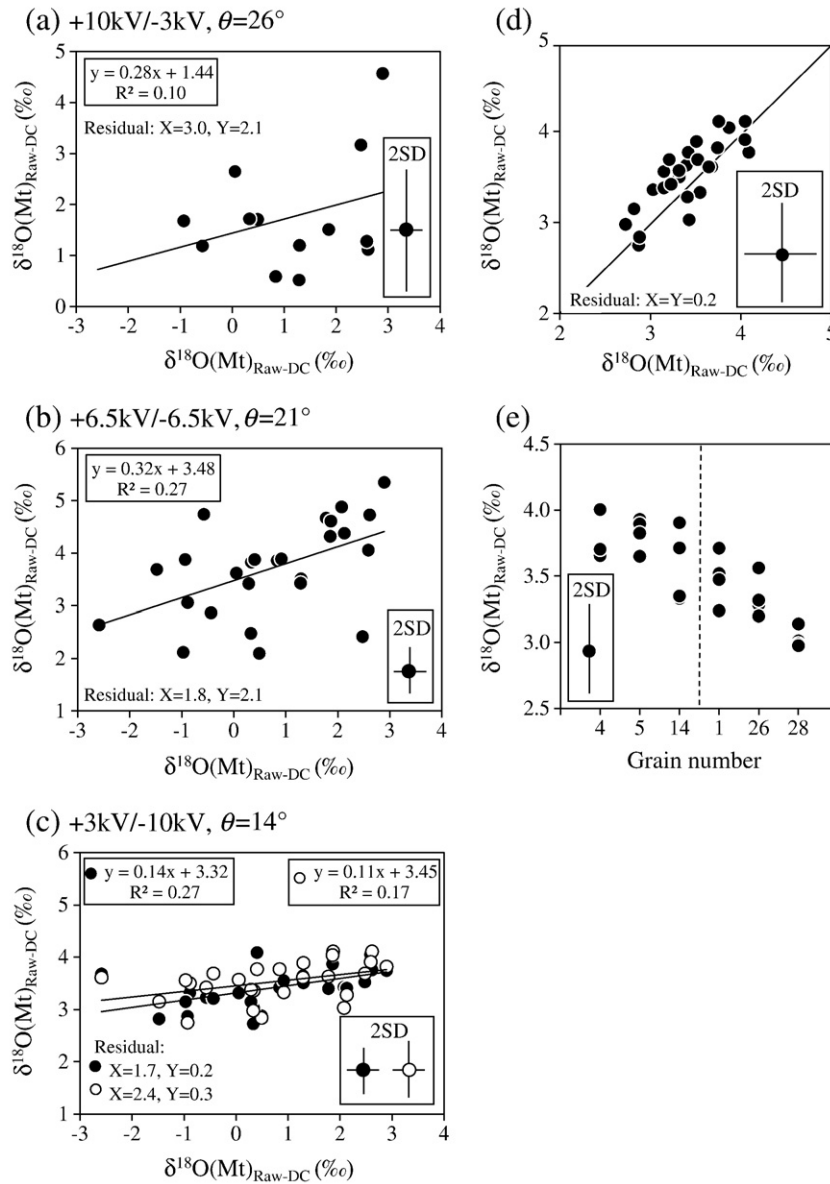


Fig. 8. Results of experiment 4 intended to improve precision in measured $\delta^{18}\text{O}$ for magnetite. 2SD is shown for bracketing UWQ-1 quartz standard analyses at the respective analytical procedures. 13 to 26 grains of magnetite 5830 with different crystal orientations have a grain-to-grain precision of $\pm 2.5\%$ to $\pm 2.9\%$ (2SD) (X-axes, Fig. 8a–c). The incident Cs^+ beam angle (θ) is calculated to be 26, 21, and 14° respectively from normal to the sample surface at a constant total impact energy of 13 keV (Fig. 8a–c). (a) For +10 kV/–3 kV analysis (see text), the grain-to-grain precision improves slightly, from $\pm 2.5\%$ to $\pm 2.2\%$ (2SD, $n = 13$). (b) For +6.5 kV/–6.5 kV analysis, the grain-to-grain precision improves from $\pm 2.9\%$ to $\pm 1.8\%$ (2SD, $n = 26$). (c) For +3 kV/10 kV analysis, the grain-to-grain precision shows the most improvement from $\pm 2.9\%$ to $\pm 0.8\%$ (2SD, $n = 26$). (d) SIMS analyses at +3 kV/10 kV analysis are shown from the 1st session (X-axis) and 2nd session (Y-axis) for the same magnetite grains at the same respective crystal orientations, and residuals are within the 2SD ($\pm 0.3\%$) of the bracketing quartz standard for an X = Y line. (e) Multiple measurements in single grains of magnetite at +3 kV/–10 kV analysis have an average precision of $\pm 0.3\%$ (2SD, $n \geq 3$).

magnetite is $\pm 0.3\%$ (2SD, $n = 6$). However there is still a consistent $\pm 0.5\%$ difference from grain-to-grain that correlates with crystal orientation of the magnetite sample.

4.4. SIMS analyses of $\delta^{18}\text{O}$ for hematite

Multiple analyses for hematite 09H1 (+10 kV/–10 kV analysis, deep-pit mode) show variation in measured $\delta^{18}\text{O}$ with crystal orientation, and the grain-to-grain precision in $\delta^{18}\text{O}(\text{Hem})_{\text{Raw-DC}}$ is $\pm 2.1\%$ (2SD, $n = 18$). In single grains of hematite analyzed three or more times, the average precision in measured $\delta^{18}\text{O}$ is $\pm 0.3\%$ ($n = 6$), identical to that obtained for the quartz standard. Pit depths are 2 μm , measured by white light profilometer. Because the grain-to-grain precision in measured $\delta^{18}\text{O}$ for magnetite 5830 was improved in experiment 4 (+3 kV/–10 kV analysis), the same procedure was applied to hematite 09H1.

Fig. 9a shows values of $\delta^{18}\text{O}(\text{Hem})_{\text{Raw-DC}}$ at +10 kV/–10 kV analysis plotted for individual grains of hematite. Seventeen to twenty grains of hematite were analyzed in the same epoxy mount at azimuths of 000° (white circles) and 180° (black circles). The grain-to-grain precision in measured $\delta^{18}\text{O}$ for hematite is $\pm 2.1\%$ (2SD, $n = 20$) at 000° and $\pm 3.0\%$ (2SD, $n = 17$) at 180° while the average precision in single grains is $\pm 0.3\%$. The average $\delta^{18}\text{O}_{\text{Raw-DC}}$ value is -0.4% for analyses made at 000° and -0.9% at 180° , reflecting differences in crystal orientations of sample grains for small data sets.

Fig. 9b shows values of $\delta^{18}\text{O}(\text{Hem})_{\text{Raw-DC}}$ at +10 kV/–10 kV (X-axis) and +3 kV/–10 kV (Y-axis) analysis. The grain-to-grain precision in measured $\delta^{18}\text{O}$ for hematite improves from $\pm 2.1\%$ to $\pm 1.0\%$ ($n = 18$) respectively. The slope of a linear fit to the data is 0.34, there is a relatively good correlation ($R^2 = 0.55$), and residuals are low ($X = 0.8$, $Y = 0.3$). Pit depths are 0.4 μm , measured by white light profilometer. Additionally,

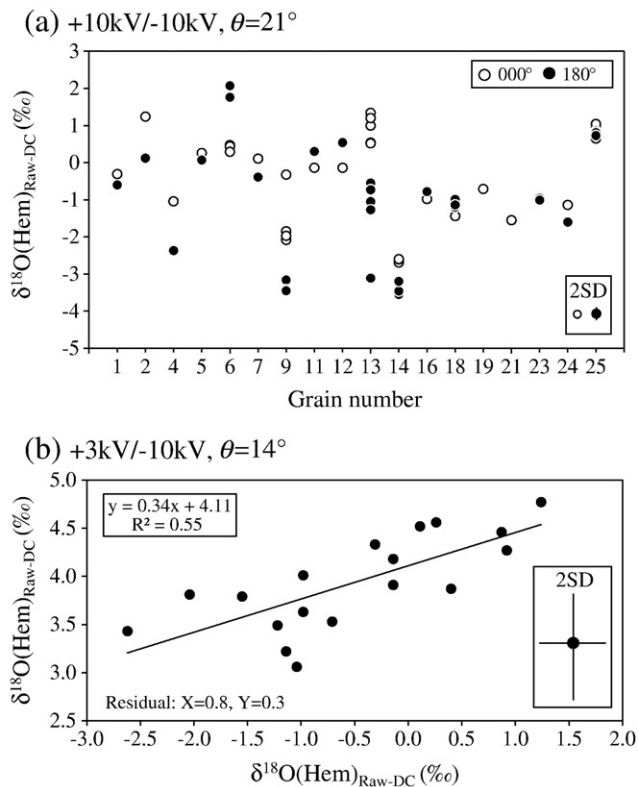


Fig. 9. (a) Results for 17 to 20 grains of hematite at routine +10 kV/–10 kV analysis and azimuths of 000° (white circles) and 180° (black circles). 2SD is shown for bracketing UWQ-1 quartz standard analyses at the respective analytical procedures. Precision from grain-to-grain of hematite is $\pm 2.1\%$ (2SD, $n=20$) at 000° and is $\pm 3.0\%$ (2SD, $n=17$) at 180° while the average precision in single grains is $\pm 0.3\%$ for both. The average $\delta^{18}\text{O}(\text{Hem})_{\text{Raw-DC}}$ value is -0.4% for analyses made at 000° and -0.9% at 180°, reflecting differences in crystal orientations of sample grains for small data sets. (b) Values of $\delta^{18}\text{O}(\text{Hem})_{\text{Raw-DC}}$ are plotted for routine +10 kV/–10 kV analysis (X-axis) and +3 kV/–10 kV analysis (Y-axis). 2SD is shown for bracketing UWQ-1 quartz standard analyses at the respective analytical procedures. The grain-to-grain precision of $\delta^{18}\text{O}(\text{Hem})_{\text{Raw-DC}}$ for hematite is $\pm 2.1\%$ (X-axis) and improves to $\pm 1.0\%$ (Y-axis) (2SD, $n=18$).

the average precision for single grains of hematite analyzed three or more times is $\pm 0.3\%$ (2SD, $n=6$) at +3 kV/–10 kV analysis, identical to that obtained at +10 kV/–10 kV analysis and for the quartz standard in both.

5. Discussion

5.1. Reducing variation in instrumental bias

Fig. 10 shows SIMS analyses of magnetite plotted for the incident Cs^+ beam angle (X-axis) and precision (2SD) in measured $\delta^{18}\text{O}$ (Y-axis). This study reports a precision in measured $\delta^{18}\text{O}$ of $\pm 2\text{--}3\%$ at 20 keV (+10 kV/–10 kV analysis) using a CAMECA IMS-1280 whereas Lyon et al. (1998) obtained a precision of $\sim \pm 5\%$ in measured $\delta^{18}\text{O}$ for magnetite at a total impact energy of 18 keV (+10 kV/–8 kV analysis) using an Isolab 54. The primary axis angle is 30° for the IMS-1270 and -1280 but is larger, 45°, for the Isolab 54. The primary beam is bent inwards towards normal to the sample surface by the opposite polarity of the primary and secondary voltages and near-sample potential fields. As a result, the incident Cs^+ beam angle is 21° at +10 kV/–10 kV analysis whereas it is 32° at the +10 kV/–8 kV analytical procedure used by Lyon et al. (1998) from Eq. (1).

A power law curve fit to magnetite analyses at 13 keV (experiment 4, closed circles) shows a strong correlation between the incident Cs^+ beam angle and precision in measured $\delta^{18}\text{O}$ ($R^2=0.72$, Fig. 10). Similarly, a power law fit to magnetite analyses at 20 keV in this study (closed squares) and that obtained by Lyon et al. (1998) scaled from 18 to 20 keV

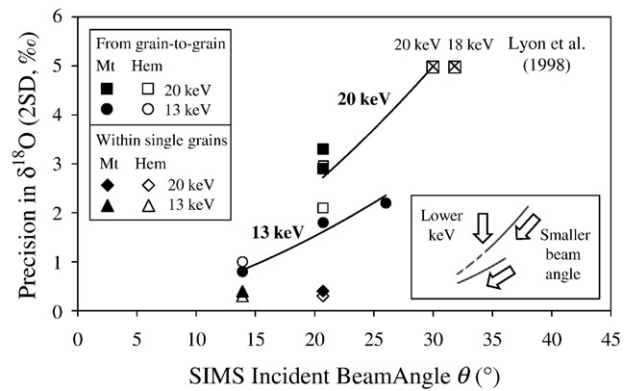


Fig. 10. The SIMS incident Cs^+ beam angle from normal of the sample surface (X-axis) is plotted against the precision in measured $\delta^{18}\text{O}$ values (Y-axis) for SIMS analyses of magnetite (closed symbols) and hematite (open symbols). In experiment 4, for magnetite analyses, the incident Cs^+ beam angle (θ) was varied from 26 to 14° (total 13 keV, closed circles), and a power law fit to these data shows a strong correlation ($R^2=0.97$). Similarly, a power law fit to analyses of magnetite at 20 keV in this study (checked squares) and that obtained by Lyon et al. (1998) scaled from 18 to 20 keV (checked squares) shows a good correlation ($R^2=0.72$). Spot-to-spot reproducibility for individual grains of magnetite and hematite of $\pm 0.4\%$ and $\pm 0.3\%$ respectively is plotted at 20 keV (diamonds) and 13 keV (triangles) for reference with no crystal orientation effects. Reducing both the total impact energy and the incident Cs^+ beam angle significantly improves the precision in measured $\delta^{18}\text{O}$. (inset)

(checked squares) shows a good correlation ($R^2=0.72$, Fig. 10). Thus, we find that precision in measured $\delta^{18}\text{O}$ for magnetite is significantly improved by reducing both the total impact energy and the incident Cs^+ beam angle from normal to the sample surface (Fig. 10 inset).

Further, precision in measured $\delta^{18}\text{O}$ for hematite at 20 keV (+10 kV/–10 kV analysis, open squares) and 13 keV (+3 kV/–10 kV analysis, open circle) overlap with values obtained for magnetite in this study. Precision in measured $\delta^{18}\text{O}$ in single grains is $\pm 0.4\%$ for magnetite and $\pm 0.3\%$ for hematite at 20 keV (diamonds) and 13 keV (triangles). This is the precision we would expect for these minerals in the absence of crystal orientation effects. Precision in measured $\delta^{18}\text{O}$ values is limited by counting statistics, and oxygen isotope analyses have an internal standard error (2SE) of $\pm 0.3\%$ at WiscSIMS.

5.2. Hypothesis for variation in bias due to crystal orientation effects

Real sample heterogeneity and magnetism of magnetite grains have been excluded as causes of variation in measured $\delta^{18}\text{O}$ and thus instrumental bias. We now consider crystal orientation effects including channeling and focusing.

Channeling of primary ions occurs when the incident angle of the primary Cs^+ beam is parallel to the set of directions $\langle uv0 \rangle$, from [110] to [100], in magnetite (Fig. 1a). Extensive channeling would be expected to attenuate secondary ion yield, which varies by $\sim 7\%$ for $\delta^{18}\text{O}$ in magnetite ($R^2=0.2$, Supplemental Table A2), but varies by 18% for $\delta^{34}\text{S}$ in sphalerite ($R^2=0.8$, Kozdon et al., 2010). Yet, no correlation is seen for magnetite when secondary ion yield is contoured on the standard triangle, which we interpret to mean that channeling is not likely a direct cause of variation in bias. The magnitude of channeling is lower for magnetite than sphalerite potentially due to differences between their crystal structures, face-centered cubic and diamond-centered cubic respectively.

Focusing of secondary ions takes place along or between planes of oxygen atoms parallel to the Cs^+ beam direction, eg., $\langle uv0 \rangle$. Focusing occurs when momentum and/or ions are transferred into or between rows and planes of atoms and results in the preferential emission of secondary ions (Fig. 1b). If focusing was responsible for variation in bias, ejection of ^{18}O or ^{16}O ions may occur along preferred crystal orientations, eg. $\langle uv0 \rangle$. This would potentially result in a trend of decreasing or increasing measured $\delta^{18}\text{O}$ values over the course of analysis, which is not

seen (Supplemental Fig. A4). Thus preferential ejection of one isotope due to focusing is also not likely a direct cause of variation in bias.

We hypothesize that channeling and focusing are not direct causes of variation in bias, yet high measured $\delta^{18}\text{O}$ values are consistently obtained when the incident Cs^+ beam is parallel to $\langle uvO \rangle$, preferred channeling and focusing directions for magnetite. Variation in bias is reduced at lower total impact energy, which is consistent with studies that show differences between crystal orientations for sputtered ions from metals and semiconductors are diminished at lower keV (Roosendaal, 1981). Variation in bias is further reduced at smaller incident beam angles from normal to the sample surface, which suggests that focused secondary ions are preferentially emitted parallel to the Cs^+ beam direction. Secondary ions are accelerated by the voltage potential between the sample and the extraction plate and are subject to the equipotential surfaces of the electrostatic field parallel to the sample surface. Thus, we hypothesize that variation in bias is caused by the electrostatic field acting upon the trajectories of focused secondary ions resulting in preferential selection of the light isotope (^{16}O) (Fig. 1c).

5.3. Evaluating crystal orientation effects

Many minerals have not been evaluated for possible crystal orientation effects during isotope ratio analysis. We propose that a difference between spot-to-spot reproducibility in single grains and from grain-to-grain provides a practical test. To evaluate this, a grain mount should be prepared where grains are mounted with a range of crystal orientations. If precision in single grains is significantly better than grain-to-grain precision, variation in bias due to crystal orientation effects is strongly suggested, but a coincidental distribution of heterogeneity still needs to be evaluated. To differentiate between sample heterogeneity and crystal orientation effects, the grain mount can be rotated in the sample holder by a proscribed amount, e.g., by 90° , for reanalysis of the same grains. If the analyzed isotope ratios for individual grains are different after rotation, but still precise for multiple analyses in single grains, crystal orientation effects are demonstrated. Conversely, if the analyzed isotope ratio does not change upon rotation, then there is no orientation effect at the measured level of precision.

To date, crystal orientation effects have been demonstrated only for $\delta^{18}\text{O}$ in magnetite and hematite, $\delta^{56}\text{Fe}$ in magnetite, and $\delta^{34}\text{S}$ in sphalerite and galena (this study; Kita et al., 2010; Kozdon et al., 2010). At WiscSIMS, we have obtained grain-to-grain precision better than ± 0.3 to 0.5% (2SD) in $\delta^{18}\text{O}$ for the garnet, carbonate, feldspar, pyroxene, and olivine groups, quartz, zircon, Mg–Al spinel, chromite, kyanite, sphene, melilite, and hibonite thus no orientation effects are indicated (Valley and Kita 2009). However, each lab should evaluate these effects as they can vary for different analytical conditions and instruments.

5.4. Crystal orientation effects by SIMS

The new understanding of crystal orientation effects for analysis of stable isotope ratios can lead to improved results in published studies. For instance, oxygen isotope ratios by SIMS are important for the study of small magnetite grains in ordinary chondrites (Choi et al., 1997, 1998, 2000; Greenwood et al., 2000; Choi and Wasson, 2003; Hsu et al., 2006; Yurimoto et al., 2008). These studies report a spot-to-spot reproducibility of ± 2 – 3% (2SD) and variable ranges in $\delta^{18}\text{O}$ for magnetite from 3% to 16%, part of which is due to crystal orientation effects. A spot-to-spot reproducibility of ± 2 – 3% in $\delta^{18}\text{O}$ for magnetite masks crystal orientation effects with a grain-to-grain precision of ± 2 – 3% . By utilizing sub-‰ precision and the improved analytical procedures documented in this study (lower total impact energy and a smaller primary beam incident angle), precision and accuracy of these analyses can be improved, and this may lead to a better understanding of the origin of magnetite in chondrites.

Improved precision in SIMS analysis of $\delta^{18}\text{O}$ for magnetite will also result in more accurate and precise temperatures using quartz-

magnetite $\delta^{18}\text{O}$ thermometry. At $T=500^\circ\text{C}$, precision improves three-fold, from $\Delta T = +112/-78^\circ\text{C}$ ($\pm 2.5\%$, $+10\text{kV}/-10\text{kV}$ analysis) to $\Delta T = +31/-28^\circ\text{C}$ ($\pm 0.8\%$, $+3\text{kV}/-10\text{kV}$ analysis), using the well-calibrated oxygen isotope thermometer of Clayton and Kieffer (1991).

As precision in isotope ratio analyses by SIMS improves further and other isotope systems are studied in detail, it is likely that other minerals will be found that exhibit variation in bias with crystal orientation. Kozdon et al. (2010) showed that sulfur isotopes ($\delta^{34}\text{S}$) vary in natural sphalerite samples and are correlated with $\langle uvw \rangle$, from [111] to [110], preferred channeling and focusing directions for sphalerite. Precision in measured $\delta^{34}\text{S}$ is $\pm 0.3\%$ (2SD) in single grains of sphalerite, identical to that obtained for homogeneous chalcopyrite (CuFeS_2) and pyrrhotite (Fe_{1-x}S) samples and close to precision of $\pm 0.2\%$ obtained for pyrite (FeS_2). At $+10\text{ kV}/-10\text{ kV}$ analysis in deep-pit mode, the grain-to-grain precision in measured $\delta^{34}\text{S}$ for sphalerite is significantly worse ($\pm 1.7\%$, Kozdon et al., 2010), but improves to $\pm 0.6\%$ in shallow-pit mode and for $+3\text{ kV}/-10\text{ kV}$ analysis (Kozdon et al., 2010). Galena (PbS) was also found to show crystal orientation effects for $\delta^{34}\text{S}$ by SIMS although due to perfect cleavage along {100}, grains may inadvertently be mounted in preferred orientation and these effects may be obscured.

Iron isotope ratios ($\delta^{56}\text{Fe}$) have been analyzed by SIMS in natural magnetite samples from Isua, SW Greenland (Whitehouse and Fedo, 2007). Those authors report a range in $\delta^{56}\text{Fe}$ of up to 2‰ in individual 1 mm rock chips and a total range of 3‰ in all samples, the full range of iron isotope ratios documented in BIFs (Johnson et al., 2008). Whitehouse and Fedo (2007) conclude that variability of $\delta^{56}\text{Fe}$ at the mm-scale reflects diagenetic zonation preserved despite amphibolite facies metamorphism. Further, they report a spot-to-spot reproducibility of $\pm 0.4\%$ (2SD) for 8 or more analyses on individual grains of the magnetite standard LP204-1, not including an additional $\pm 0.25\%$ uncertainty from grain-to-grain. Herrick (2007) analyzed micro-drilled ~ 1 mg aliquots of magnetite powder from samples in the same metasedimentary belt by multi-collector inductively coupled plasma mass spectrometry (MC-ICP-MS) with a reproducibility in $\delta^{56}\text{Fe}$ of $\pm 0.1\%$ (2SD) and found that individual mm-layers of magnetite are homogeneous in $\delta^{56}\text{Fe}$ to 0.1‰ with a total range of 0.8‰ in all samples. Kita et al. (2010) evaluated a different magnetite, 08-BI-12 (Biwabik, Minnesota), by SIMS and reported a grain-to-grain precision in measured $\delta^{56}\text{Fe}$ of $\pm 0.6\%$ (2SD), while precision in single grains is ± 0.1 – 0.2% . Analyses of the same sample by MC-ICP-MS were performed with precision in $\delta^{56}\text{Fe}$ of $\pm 0.07\%$ (2SD). Kita et al. (2010) proposed that variation in measured $\delta^{56}\text{Fe}$ for this homogeneous sample is caused by crystal orientation effects. Thus, it is likely that the range in $\delta^{56}\text{Fe}$ of 2‰ for individual Isua samples measured by SIMS with a CAMECA IMS-1270 (Whitehouse and Fedo, 2007) is at least in part caused by crystal orientation effects.

Crystal orientation effects on measurements of $^{206}\text{Pb}/^{238}\text{U}$ in baddeleyite by SIMS have also been reported. Wingate and Compston (2001) obtained a precision of $\pm 10\%$ in $^{206}\text{Pb}/^{238}\text{U}$ from grain-to-grain of baddeleyite with a spot-to-spot reproducibility of ± 1 – 2% using a SHRIMP II. In contrast, Schmitt et al. (2010) found that, for randomly mounted grains of the same baddeleyite samples, the grain-to-grain precision is better, ± 2 – 4% , using an IMS-1270 with a spot-to-spot reproducibility of ± 1 – 2% . Those authors attribute the improved precision to increased ionization of ^{206}Pb due to use of an oxygen flood gun during analysis and a UO_2^+/U^+ -based calibration. However, the primary axis angle is 45° for the SHRIMP II but is 30° for the IMS-1270. Thus improvement in the precision of $^{206}\text{Pb}/^{238}\text{U}$ in baddeleyite by SIMS may also be due to the smaller impact angle of the primary beam of the IMS-1280 ($\theta=22^\circ$, $+13\text{ kV}/-10\text{ kV}$ analysis) than the SHRIMP II ($\theta=30^\circ$, $+10\text{ kV}/-10\text{ kV}$ analysis) and may be further improved by analyzing at lower total impact energy and a smaller primary beam angle.

6. Conclusions

In situ high precision analysis of oxygen isotopes by SIMS exhibits variation in instrumental bias in $\delta^{18}\text{O}$ for magnetite and hematite

due to crystal orientation effects. Failure to recognize this effect may result in precise, but inaccurate analyses of single crystals of magnetite or hematite, but this effect has not yet been found for $\delta^{18}\text{O}$ in other minerals. The average spot-to-spot reproducibility of $\delta^{18}\text{O}$ is $\pm 0.4\%$ (2SD) in single grains of magnetite, close to $\pm 0.3\%$, that obtained for homogeneous standards of many silicate minerals. In contrast, the average precision from grain-to-grain of magnetite is $\pm 2\text{--}3\%$ (2SD) for routine $+10\text{ kV}/-10\text{ kV}$ analysis. High $\delta^{18}\text{O}$ values are obtained when the incident Cs^+ beam angle is parallel to $\langle uv0 \rangle$, from $[110]$ to $[100]$, preferred channeling and focusing directions for magnetite. Four analytical experiments were employed to improve precision in measured $\delta^{18}\text{O}$. The best results were obtained at $-3\text{ kV}/+10\text{ kV}$ analysis (total impact energy of 13 keV), with an incident Cs^+ beam angle of 14° from normal to the sample surface. The grain-to-grain precision in $\delta^{18}\text{O}(\text{Mt})_{\text{Raw-DC}}$ of magnetite improves from $\pm 2.9\%$ to $\pm 0.8\%$ (2SD, $n=26$) for $+10\text{ kV}/-10\text{ kV}$ and $+3\text{ kV}/-10\text{ kV}$ analysis respectively. Similar results were obtained for hematite, and grain-to-grain precision in $\delta^{18}\text{O}(\text{Hem})_{\text{Raw-DC}}$ improves from $\pm 2.1\%$ to $\pm 1.0\%$ (2SD, $n=18$) for $+10\text{ kV}/-10\text{ kV}$ and $+3\text{ kV}/-10\text{ kV}$ analysis respectively. Precision in measured $\delta^{18}\text{O}$ for magnetite and hematite is significantly improved for smaller values of both the total impact energy and the incident Cs^+ beam angle. The ability to minimize crystal orientation effects will permit more accurate standardization of oxygen isotope ratios.

Acknowledgments

We thank Brian Hess for sample preparation, Jim Kern for technical assistance and Takayuki Ushikubo, Ian Lyon, John Saxton, and Paul Voyles for many fruitful discussions. Yuichi Morishita at the Geological Survey of Japan provided sample M34572-A, Brian Beard provided sample 08-BI-12, and the UW-Madison Geology Museum provided sample 09H1. Reviews by Hisayoshi Yurimoto and John Ferry substantially improved this paper. This study was funded by the NASA Astrobiology Institute, NSF-EAR (0509639, 0838058) and DOE (93ER 14389). WiscSIMS is partly supported by NSF-EAR (0319230, 0516725, 0744079).

Appendix A. Supplementary data

Supplementary data associated with this article can be found, in the online version, at [doi:10.1016/j.chemgeo.2010.06.012](https://doi.org/10.1016/j.chemgeo.2010.06.012).

References

- Armstrong, J.T., 1998. Quantitative analysis of silicates and oxide minerals: comparison of Monte Carlo, ZAF and phi-rho-z procedures. In: Newbury, D.E. (Ed.), *Microbeam Analysis*. San Francisco Press, San Francisco, pp. 239–246.
- Behrisch, R., Eckstein, W., 2007. Introduction and overview. *Sputtering by Particle Bombardment*. In: Behrisch, R., Eckstein, W. (Eds.), *Topics in Applied Physics*, 110. Springer-Verlag, New York, pp. 1–20.
- Benninghoven, A., 1994. Chemical analysis of inorganic and organic surfaces and thin films by static time-of-flight secondary ion mass spectrometry (TOF-SIMS). *Angewandte Chemie International Edition in English* 33 (10), 1023–1043.
- Benninghoven, A., Rüdener, F.G., Werner, H.W., 1987. Secondary Ion Mass Spectrometry: Basic Concepts, Instrumental Aspects, Applications and Trends. *Chemical Analysis*. J. Wiley and Sons, New York, 1227 pp.
- Cameca, 2004. *Cameca IMS 1270/80 User's Guide*. 510 pp.
- Choi, B.-G., Wasson, J.T., 2003. Microscale oxygen isotopic exchange and magnetite formation in the Ningqiang anomalous carbonaceous chondrite. *Geochimica et Cosmochimica Acta* 67 (23), 4655–4660.
- Choi, B.-G., McKeegan, K.D., Leshin, L.A., Wasson, J.T., 1997. Origin of magnetite in oxidized CV chondrites: in situ measurement of oxygen isotope compositions of Allende magnetite and olivine. *Earth and Planetary Science Letters* 146 (1–2), 337–349.
- Choi, B.-G., McKeegan, K.D., Krot, A.N., Wasson, J.T., 1998. Extreme oxygen isotope compositions in magnetite from unequilibrated ordinary chondrites. *Nature* 392 (9), 577–579.
- Choi, B.-G., Krot, A.N., Wasson, J.T., 2000. Oxygen isotopes in magnetite and fayalite in CV chondrites Kaba and Mokoia. *Meteorites and Planetary Science* 35, 1239–1248.
- Clayton, R.N., Kieffer, S.W., 1991. Stable isotope thermometry at high temperatures. Oxygen isotopic thermometer calibrations. In: Taylor, H.P., O'Neil, J.R., Kaplan, I.R. (Eds.), *Geochemical Society Special Publication*, 3, pp. 3–10.
- CrystalMaker, 2008. *CrystalMaker® 8.2*. PO Box 183, Bicester, Oxfordshire OX26 3TA, England.
- Donovan, J.J., Kremser, D., Fournelle, J.H. (Eds.), 2010. *Probe for EPMA v. 8.24 User's Guide and Reference*, Enterprise Edition. 398 pp.
- Eckstein, W., 2007. Sputtering yields. *Sputtering by Particle Bombardment*. In: Behrisch, R., Eckstein, W. (Eds.), *Topics in Applied Physics*, 110. Springer-Verlag, New York.
- Eiler, J.M., Valley, J.W., Graham, C.M., Baumgartner, L.P., 1995a. The oxygen isotope anatomy of a slowly cooled metamorphic rock. *American Mineralogist* 80 (7–8), 757–764.
- Eiler, J.M., Valley, J.W., Graham, C.M., Baumgartner, L.P., 1995b. Ion microprobe evidence for the mechanisms of stable isotope retrogression in high-grade metamorphic rocks. *Contributions to Mineralogy and Petrology* 118 (4), 365–378.
- Eiler, J.M., Graham, C.M., Valley, J.W., 1997. SIMS analysis of oxygen isotopes: matrix effects in complex minerals and glasses. *Chemical Geology* 138, 221–244.
- Eiler, J.M., Schiano, P., Valley, J.W., Kita, N.T., Stolper, E.M., 2007. Oxygen-isotope and trace element constraints on the origins of silica-rich melts in the subarc mantle. *Geochemistry Geophysics Geosystems* 8 (9), Q09012 (22 pp.).
- Galouchko, V., 2008. *3DFieldPro v.2.2.2*.
- Gnaser, H., 2007. Energy and angular distributions of sputtered species. *Sputtering by Particle Bombardment*. In: Behrisch, R., Eckstein, W. (Eds.), *Topics in Applied Physics*, 110. Springer-Verlag, New York, pp. 231–328.
- Greenwood, J.P., Rubin, A.E., Wasson, J.T., 2000. Oxygen isotopes in R-chondrite magnetite and olivine: links between R chondrites and ordinary chondrites. *Geochimica et Cosmochimica Acta* 64 (22), 3897–3911.
- Herrick, M.J., 2007. Isotopic studies of the 3.7–3.8 Ga Isua Banded Iron Formation provide insight into early Archean geochemical cycles. MS Thesis, UW-Madison, Madison, WI.
- Hervig, R.L., Williams, P., Thomas, R.M., Schauer, S.N., Steele, I.M., 1992. Microanalysis of oxygen isotopes in insulators by secondary ion mass spectrometry. *International Journal of Mass Spectrometry and Ion Processes* 120 (1–2), 45–63.
- Hsu, W., Guan, Y., Hua, X., Wang, Y., Leshin, L.A., Sharp, T.G., 2006. Aqueous alteration of opaque assemblages in the Ningqiang carbonaceous chondrite: evidence from oxygen isotopes. *Earth and Planetary Science Letters* 243, 107–114.
- Johnson, C.M., Beard, B.L., Roden, E.E., 2008. The iron isotope fingerprints of redox and biogeochemical cycling in modern and ancient earth. *Annual Review of Earth and Planetary Sciences* 36, 457–493.
- Kelly, J.L., Fu, B., Kita, N.T., Valley, J.W., 2007. Optically continuous silcrete quartz cements of the St. Peter Sandstone: high precision oxygen isotope analysis by ion microprobe. *Geochimica et Cosmochimica Acta* 71 (15), 3812–3822.
- Kita, N.T., Ikeda, Y., Togashi, S., Liu, Y.Z., Morishita, Y., Weisberg, M.K., 2004. Origin of ureilites inferred from a SIMS oxygen isotopic and trace element study of clasts in the Dar al Gani 319 polymict ureilite. *Geochimica et Cosmochimica Acta* 68 (20), 4213–4235.
- Kita, N.T., Ushikubo, T., Fu, B., Valley, J.W., 2009. High precision SIMS oxygen isotope analysis and the effect of sample topography. *Chemical Geology* 264 (1–4), 43–57.
- Kita, N.T., Huberty, J.M., Kozdon, R., Beard, B.L., Valley, J.W., 2010. High precision SIMS oxygen, sulfur and iron stable isotope analyses of geological materials: accuracy, surface topography and crystal orientation. *Surface and Interface Analysis*. [doi:10.1002/sia.3424](https://doi.org/10.1002/sia.3424).
- Kozdon, R.K., Kita, N.T., Huberty, J.M., Fournelle, J.H., Valley, J.W., 2010. In situ sulfur isotope analysis of sulfide minerals by SIMS: precision and accuracy, with application to thermometry of 3.5 Ga Pilbara cherts. *Chemical Geology* 275 (3–4), 243–253.
- Lyon, I.C., Saxton, J.M., Cornah, S.J., 1998. Isotopic fractionation during secondary ionisation mass spectrometry: crystallographic orientation effects in magnetite. *International Journal of Mass Spectrometry and Ion Processes* 172 (1–2), 115–122.
- Rasband, W., 2010. *ImageJ 1.42q*. National Institutes of Health, USA.
- Riciputi, L.R., Paterson, B.A., Ripperdan, R.L., 1998. Measurement of light stable isotope ratios by SIMS: matrix effects for oxygen, carbon, and sulfur isotopes in minerals. *International Journal of Mass Spectrometry* 178 (1–2), 81–112.
- Robinson, M.T., 1981. Theoretical aspects of monocrystal sputtering. *Sputtering by Particle Bombardment*. In: Behrisch, R. (Ed.), *Topics in Applied Physics*, 47. Springer-Verlag, New York, pp. 73–144.
- Röller, K., Trepmann, C.A., 2008. *Stereo32 v. 1.0.1*. Ruhr-Universität Bochum, Institut für Geologie, Mineralogie & Geophysik, Bochum, Germany.
- Roosendaal, H.E., 1981. Sputtering yields of single crystalline targets. *Sputtering by Particle Bombardment*. In: Behrisch, R. (Ed.), *Topics in Applied Physics*, 47. Springer-Verlag, New York, pp. 219–266.
- Schmitt, A.K., Chamberlain, K.R., Swapp, S.M., Harrison, T.M., 2010. In situ U–Pb dating of micro-baddeleyite by secondary ion mass spectrometry. *Chemical Geology* 269 (3–4), 386–395.
- Sitzman, S.D., Banfield, J.F., Valley, J.W., 2000. Microstructural characterization of metamorphic magnetite crystals with implications for oxygen isotope distribution. *American Mineralogist* 85 (1), 14–21.
- Valaas Hyslop, E., Valley, J.W., Johnson, C.M., Beard, B.L., 2008. The effects of metamorphism on O and Fe isotope compositions in the Biwabik Iron Formation, northern Minnesota. *Contributions to Mineralogy and Petrology* 155, 313–328.
- Valley, J.W., 2001. Stable isotope thermometry at high temperatures. *Stable Isotope Geochemistry*. In: Valley, J.W., Cole, D.R. (Eds.), *Stable Isotope Geochemistry, Reviews In Mineralogy and Geochemistry*, 43, pp. 365–414.
- Valley, J.W., Graham, C.M., 1991. Ion microprobe analysis of oxygen isotope ratios in granulite facies magnetites: diffusive exchange as a guide to cooling history. *Contributions to Mineralogy and Petrology* 109 (1), 38–52.
- Valley, J.W., Graham, C.M., 1993. Cryptic grain-scale heterogeneity of oxygen isotope ratios in metamorphic magnetite. *Science* 259 (5102), 1729–1733.
- Valley, J.W., Kita, N.T., 2009. In situ oxygen isotope geochemistry by ion microprobe. In: Fayek, M. (Ed.), *Mineralogical Association of Canada Short Course 41: Secondary Ion Mass Spectrometry in the Earth Sciences*, pp. 19–63.
- Valley, J.W., O'Neil, J.R., 1984. Fluid heterogeneity during granulite facies metamorphism in the Adirondacks: stable isotope evidence. *Contributions to Mineralogy and Petrology* 85 (2), 158–173.

- Valley, J.W., Kitchen, N.E., Kohn, M.J., Niendorf, C.R., Spicuzza, M.J., 1995. UWG-2, a garnet standard for oxygen isotope ratios: strategies for high precision and accuracy with laser heating. *Geochimica et Cosmochimica Acta* 59 (24), 5223–5231.
- Valley, J.W., Graham, C.M., Harte, B., Kinny, P., Eiler, J.M., 1998. Ion microprobe analysis of oxygen, carbon, and hydrogen isotope ratios. In: McKibben, M.A., Shanks, W.C. (Eds.), *Society of Economic Geologists Reviews in Economic Geology*, 7, pp. 73–98.
- Whitehouse, M.J., Fedo, C.M., 2007. Microscale heterogeneity of Fe isotopes in >3.71 Ga banded iron formation from the Isua Greenstone Belt, southwest Greenland. *Geology* 35 (8), 719–722.
- Wingate, M.T.D., Compston, W., 2001. Crystal orientation effects during ion-microprobe U–Pb analysis of baddeleyite. *Chemical Geology* 168 (1–2), 75–97.
- Yurimoto, H., Krot, A.N., Choi, B.-G., Aléon, J., Kunihiro, T., Brearley, A.J., 2008. Oxygen isotopes of chondritic components. *Oxygen in the Solar System*. In: MacPherson, G.J. (Ed.), *Reviews in Mineralogy & Geochemistry*, 68, pp. 141–186.
- Zheng, Y.-F., 1991. Calculation of oxygen isotope fractionation in metal oxides. *Geochimica et Cosmochimica Acta* 55 (8), 2299–2307.